CONF-9806141--

The Long Range Migration of Hydrogen Through Zircaloy in Response to Tensile and Compressive Stress Gradients

B. F. Kammenzind

B. M. Berquist

R. Bajaj

P. H. Kreyns

D. G. Franklin

Presented at the Twelfth International Symposium on Zirconium in the Nuclear Industry

Toronto, Canada

June 15-18, 1998

Westinghouse Electric Company

Bettis Atomic Power Laboratory

DISCLAIMER

Abstract

Zircaloy-4, which is used widely as a core structural material in pressurized water reactors (PWR's), picks up hydrogen during service. Hydrogen solubility in Zircaloy-4 is low and zirconium hydride phases precipitate after the Zircaloy-4 lattice becomes supersaturated with hydrogen. These hydrides embrittle the Zircaloy-4, degrading its mechanical performance as a structural material. Because hydrogen can move rapidly through the Zircaloy-4 lattice, the potential exists for large concentrations of hydride to accumulate in local regions of a Zircaloy component remote from its point of entry into the component. Much has been reported in the literature regarding the long range migration of hydrogen through Zircaloy under concentration gradients and temperature gradients. Relatively little has been reported, however, regarding the long range migration of hydrogen under stress gradients. This paper presents experimental results regarding the long range migration of hydrogen through Zircaloy in response to both tensile and compressive stress gradients. The importance of this driving force for hydrogen migration relative to concentration and thermal gradients is discussed.

The Long Range Migration of Hydrogen Through Zircaloy in Response to Tensile and Compressive Stress Gradients

B. F. Kammenzind, B.M. Berquist, R Bajaj, P.H. Kreyns, and D.G. Franklin

Introduction

It has long been known that zirconium-based cladding alloys absorb hydrogen as a result of service in a pressurized water reactor (PWR) primary side environment. The absorbed hydrogen has three potential sources: the absorption of the hydrogen cathodically generated as a result of the corrosion of the cladding by the primary side water coolant [1]; the direct absorption of the hydrogen gas dissolved in PWR primary side coolants [2]; and the absorption of hydrogen resulting from corrosion by hydrogen containing gases or vapors in the internal plenum region of fuel rods [3]. Under modern PWR operating conditions, the first of these, cathodic production as a result of water corrosion of the cladding, is the primary source of the extended hydrogen pickup occurring in high burnup fuel rods.

The accumulation of hydrogen must be considered in fuel rod performance calculations. At normal reactor operating temperatures, hydrogen has limited solubility in the zirconium lattice and precipitates out of solid solution as zirconium hydride when the solid solubility is exceeded [4-10]. The precipitation of zirconium hydride embrittles the zirconium alloy cladding, thus reducing its fracture toughness [11, 12] and tensile ductility [11, 13]. Also the hydride is less dense than the metal [14] and can cause fuel rod swelling and distortion. Finally, laboratory studies [15-17] and fuel-rod cladding corrosion modeling [18, 19] suggest that hydride accumulation at the outer surface of fuel rod cladding may be responsible for the large increase in cladding corrosion observed in the final cycle of extended-burnup fuel rods.

Because hydrogen diffuses rapidly through zirconium alloys as an interstitial atom in the zirconium lattice [4, 5, 6, 20-22], it is not sufficient in fuel rod performance calculations to merely account for the

increase in the uniform hydrogen concentration of the cladding as a result of the corrosion-induced hydrogen absorption process. Hydrogen segregation within the cladding, which can lead to large local hydride accumulation, also must be considered. A previous paper [1] provided the basis for characterizing and modeling hydrogen diffusion through Zircaloy-4 in response to concentration and temperature gradients. This paper builds on the previous, and describes experimental work to characterize and model hydrogen diffusion through Zircaloy-4 in response to both applied-stress and self-stress gradients within the cladding. The experimental work reported herein demonstrates that significant hydrogen migration occurs in Zircaloy in response to stress gradients, in the presence of thermal cycling. The driving force of the stress induced migration is small, however; significantly less than that created by thermal gradients. Before describing the experimental work, a review of theoretical models for stress induced hydrogen migration is first provided, as it is the basis for the experimental work described subsequently.

Analytical Modeling

Experimental and analytical modeling work performed at the Bettis Laboratory to describe the migration of hydrogen through the Zircaloy lattice in response to both solid-solution hydrogen concentration gradients and thermal gradients was previously described [1]. The model accounted for the diffusion of hydrogen through the Zircaloy lattice as an interstitial impurity dissolved in solid solution. Diffusion both as a result of solid-solution concentration gradients and temperature gradients was included. The temperature dependent solid-solution solubility of hydrogen in the Zircaloy lattice, the hysteresis in the hydride dissolution and precipitation solvus, and the finite kinetics of the hydride precipitation reaction were specifically included in the analytical model. The basic modeling equations are described in Table 1. The finite element computational program used to perform the calculations (modified to accommodate a difference in the solubility limits for hydride dissolution and precipitation) is described in Reference [23]. Benchmark diffusion experiments conducted under imposed thermal gradients found the model described in Reference [1] to give good agreement with experimental observations under conditions of steep thermal

gradients (~66 C/cm) [1], but to over predict the observed hydrogen segregation under shallow thermal gradients (~7 C cm). The analytic and experimental work described herein builds on the work of Reference [1] to investigate the potential role that stress gradients (either applied or self imposed) within the Zircaloy component may play in the long-range migration of hydrogen through Zircaloy-4.

Applied Stresses

The applied stresses considered are those from sources external to the cladding, such as stresses imposed on the cladding by the swelling fuel pellets. A stress gradient within a Zircaloy component might affect hydrogen migration in two ways. First, an applied stress could influence the chemical potential of a hydrogen atom dissolved in the Zircaloy lattice. A gradient in the stress field would then directly influence hydrogen diffusion by providing another driving force for hydrogen diffusion through the zirconium lattice in addition to the solid-solution concentration gradient and thermal gradients discussed in Reference [1]. Following the treatment established by Li, Oriani, and Darken [24], the flux of the diffusing hydrogen atoms can be described by:

$$J = -D(\nabla C) - (DQ^*C/RT^2)\nabla T + (DCV/RT)\nabla\sigma_H , \quad (1)$$

with the last term accounting for the stress driven diffusion, where:

V = the partial mold volume of hydrogen dissolved in the Zircaloy lattice,

σ_H = the applied hydrostatic stress, and is positive if tensile.

All other terms are as described in Table 1.

An applied stress gradient in the material also could indirectly affect hydrogen migration by affecting the terminal solid-solution solubility (TSS) of hydrogen in the material in equilibrium with hydride dissolution and precipitation. A local increase or decrease in the solid-solution solubility can result in a solid-solution concentration gradient within the component in a two-phase α + hydride field. This can result in either a net influx or outflux of hydrogen into the region, all other factors remaining the same. As discussed in detail by

Puls [25,26], the hydride is less dense than the surrounding Zircaloy lattice, requiring work to be performed in the formation of the hydride precipitate. An applied stress, depending on its direction, can therefore be expected to either assist hydride precipitation and dissolution or oppose hydride precipitation and dissolution. Using the formulation of Reference [27], the magnitude of the effect of an applied stress on the hydrogen solvus can be described by the expression:

$$C_\sigma = C_0 \exp (\sigma_H (V - V_H)/RT) \qquad (2)$$

where:

C_σ = the stress-affected solid-solution solubility.

C_0 = the stress-free solid-solution solubility,

σ_H = the applied hydrostatic stress,

V = the partial molal volume of hydrogen dissolved in the Zircaloy lattice,

V_H = the partial molal volume associated with hydride formation.

Self Imposed Stresses

The self imposed stress considered is an extension of the above-described concept regarding the effect of an applied stress on the local solid-solution solubility. The self-stress is in response to the stress imposed on the Zircaloy lattice by the precipitation of the less dense zirconium hydride. The hydride will be in compression and the lattice near the interface in tension, in accordance with the treatment of Eshelby [28, 29]. The opposite occurs away from the hydride in the bulk of the matrix. As the number density of hydride precipitates increases within a two-phase hydride-Zircaloy region, it has been hypothesized that the Zircaloy lattice between the precipitates will be placed in an increasing state of compression. This would make the terminal solid-solution solubility of hydrogen dissolved in the lattice not only a function of temperature but also a continuous function of the amount of hydride present across the two-phase field of the phase diagram as discussed by Markowitz [30]. The envisioned mechanism by which this would occur is essentially the same as that described by equation 2.

Since the stress imposed on the lattice as a function of the hydride concentration is not known, as a first order approximation, the local solid-solution solubility can be described simply as an increasing function of the volume fraction of the precipitated hydride in the region. That is:

$$C_{sself} = C_0 (1 + k_s C_{hyd}) \quad (3)$$

where:

C_{self} -stress solid-solution solubility,

C_0 = the stress-free solid-solution solubility,

k_s = a proportionality constant, and

C_{hyd} = the local hydride concentration.

Since the local hydride concentration is also a function of the self-stress solid-solution solubility:

$$C_{hyd} = C_{tot} - C_{\sigma\,self}, \quad (4)$$

where:

C_{tot} = the total concentration of hydrogen in the region, both in solid solution and precipitated.

Equations 3 and 4 can be combined to obtain:

$$C_{\sigma self} = C_o (1 + k_s C_{tot}) / (1 + k_s C_o). \quad (5)$$

In this way, the local hydrogen solubility limit varies continuously across the two-phase field of the phase diagram, and becomes an increasing function of the total hydrogen concentration of the region. Again, the envisioned mechanism causing this is the same as that described by equation 2 above for the effect of a compressive stress on the hydrogen precipitation solvus.

Previous papers have discussed the above identified potential effects of stress gradients on hydrogen migration through zirconium alloys [24, 27, 31-35] and some have provided experimental results as to the magnitude of the stress effects [27, 30, 35-40]. However, the early experimental results were mixed, and much of the experimental work has focussed either on the reorientation of hydride platelets or

on the onset of delayed hydride cracking. Few experimental measurements of the bulk transport of hydrogen into or out of a region as a result of stress gradients are available in the literature. The remainder of this paper describes a series of experiments conducted to quantify (in terms of bulk hydrogen transport into or out of a stressed region) the magnitude of the above three mechanisms (Equations 1, 2, and 5) for stress-assisted hydrogen migration, and to compare them in relation to the concentration gradient and thermal gradient mechanisms discussed in Reference [1].

Materials

Chemistry

All experiments were performed with test specimens machined from Zircaloy-4 rolled plate product. The parent Zircaloy-4 ingot was double melted in the form of 46 cm diameter, 8000 Kg ingots. Test specimens were derived from two separate ingots; the applied-stress test specimens from ingot A and the self-stress test specimens from ingot B. The major alloying element and impurity chemistry of these two Zircaloy-4 ingots is summarized below.

Heat	Sn w/o	Fe w/o	Cr w/o	C ppm	Si ppm	O ppm	N ppm	H ppm
A	1.43	0.21	0.11	135	60	1400	40	10
B	1.49	0.20	0.11	135	60	1300	40	7

Processing

The 8000 Kg Zircaloy-4 ingots were forged into slabs at high temperature and then rolled into final product. The initial rolling operations were performed low in the alpha-plus-beta two-phase field. All final rolling operations were performed high in the single-phase alpha field. Rolling reduction operations were followed by high-temperature single-phase alpha anneals to maintain a recrystallized microstructure in the material. In terms of the "A" parameter [40], the thermal-mechanical processing, from the time of the last high-temperature beta anneal, produced an "A" of approximately 1×10^{-16}, where A is defined as:

$$A = t_i \exp(40{,}000/T_i)$$

t_i = the time of annealing step i in hrs, and

T_i = the temperature of annealing step i in degrees kelvin.

Microstructure and Tensile Properties

Zircaloy-4 processed in the above manner is in a recrystallized alpha-annealed condition. The basic microstructure as revealed by light optical microscopy is illustrated in Figure 1. The material has fine equiaxed grains with a mean diameter of approximately 12 microns. Intragranular precipitation of a fine second phase is also evident in Figure 1. The second phase is more or less randomly distributed in the metallographic plane transverse to the rolling direction, but is somewhat stringered along the rolling direction in the metallographic plane containing the rolling direction. A higher magnification Transmission Electron Microscopy (TEM) image of the material showing the intragranular nature of the second-phase precipitation is provided in Figure 2. Energy Dispersive x-ray Spectroscopy (EDS) in an Analytical Electron Microscope (AEM) identified the fine intragranular precipitates to contain primarily zirconium, iron, and chromium in the approximate proportion Zr $(Fe_{0.66}Cr_{0.33})_2$. Electron diffraction in the AEM confirmed the intragranular precipitated second phase to be the hexagonal form of the Laves phase, expected in high "A" parameter processed Zircaloy-4 [41]. The diffraction analysis confirmed the material to have a low dislocation density, as expected for fully recrystallized Zircaloy-4. The size distribution of the Laves phase precipitates, as observed via the Scanning Electron Microscope (SEM) analysis of the material, after etching utilizing the techniques of Reference [42], is consistent with previous reports of high "A" parameter Zircaloy-4 material (Figure 3). Inverse and direct pole figures produced by x-ray diffraction (XRD) and Orientation Imaging Microscopy (OIM) respectively (Figures 4 and 5) show the material to have the expected Zircaloy-4 rolling texture. Average tensile properties for this material, as determined by uniaxial tensile specimens tested in the transverse and longitudinal orientations, are provided in Figure 6.

Experimental Details

Specimen Design

Three separate test specimens were utilized to investigate the three mechanisms described by Equations 1, 2, and 5 by which a stress gradient might cause hydrogen to migrate through Zircaloy-4. To investigate whether an applied stress gradient will produce a sufficient gradient in the chemical potential of the hydrogen dissolved in the Zircaloy lattice to cause hydrogen diffusion, in accordance with equation 1, the uniaxial dog-bone shaped test specimen of Figure 7 was utilized. The gage section was designed to have a shape such that the stress in the gage section was a linear function of the axial position along the length of the gage section:

$$\sigma = ax + b = F/\pi r^2 \qquad (6)$$

where:

F = the applied load on the sample, and

r = the radius of the sample at position x.

Defining $r = r_1$ at $x = 0$ (the maxima in the radius) and $r = r_2$ at $x = h$ (the minima in the radius), the descriptive equation for the dog-bone-shaped gage section is:

$$r = [x/h \{1/r_2^2 - 1/r_1^2\} + 1/r_1^2]^{-1/2}. \qquad (7)$$

The linear stress gradient was desired to provide easy analysis of the final hydrogen migration data. Solving equation 1 for the final steady-state (J=0) hydrogen concentration profile under isothermal conditions, the final hydrogen concentration gradient through the gage section is found to be directly proportional to the stress gradient:

$$Ddc/dx = (DCV/RT)\, d\sigma_H/dx. \qquad (8)$$

Combining equation 8 with equation 6 for the dog-bone specimen of Figure 7, any measured concentration gradient in the gage section should then be linear with position:

$$Ddc/dx = (DCV/3RT)a. \qquad (9)$$

The thick low-stressed region outside the gage section served either as a source or sink for hydrogen diffusing into or out of the gage length.

To investigate whether the applied stress impacts the local solid-solution solvus for hydrogen in Zircaloy, in accordance with equation 2, the test specimens of Figure 8 were utilized. The wide flat notched tensile specimen was used in preference to the round specimen, in tension, to produce plane-strain tensile conditions in the gage section. This maximized the hydrostatic stress state difference between the gage section and the remainder of the sample. Again the thick low-stressed region of the samples outside of the gage length served either as a source or sink for hydrogen moving into or out of the gage length.

To investigate whether the local hydride concentration of Zircaloy impacts the local solid- solution solvus (self-stress), the test specimens of Figure 9 were utilized. These specimens had no provision (such as a reduced dimension gage length) for creating an applied stress gradient within the sample. Rather, the two halves of each specimen were hydrogen precharged to two different starting concentrations to create a hydrogen-concentration diffusion couple. The self-stress gradient was established by the differing hydride concentrations on the two sides of the diffusion couples at test temperature.

Hydrogen Precharging

Two techniques for hydrogen precharging of the samples were utilized. Both of the applied-stress test specimens of Figures 7 and 8 were uniformly precharged with hydrogen prior to test exposure using the gaseous procedure described in Reference [43]. The machined test samples were sealed in an evacuated quartz bulb with a predetermined mass of zirconium hydride chips. The required mass was determined through a hydrogen mass balance between the initial chip concentration and the final desired specimen concentration. The evacuated bulbs containing the specimens and the chips were annealed for 8 hrs at a temperature of 600°C to allow the hydrogen from the hydride chips to transfer to the test

specimens via the equilibrium hydrogen partial pressure difference between the two materials. The annealing temperature (600°C) was sufficient that the final hydrogen concentrations were below the hydride precipitation solvus during the anneal. The annealing time was sufficient that the precharged hydrogen could come to equilibrium through the entire thickness of the test specimens. Following the 8-hr anneal, the test specimens were furnace cooled to room temperature.

The initial hydrogen concentration gradient within the self-stress samples of Figure 9 were produced using the aqueous cathodic procedure described in Reference [44]. Brightly pickled test specimens were masked with a nonconducting lacquer to expose only those surfaces to be hydrogen precharged. The specimens were then exposed to a 1N H_2SO_4 solution, containing $NaAsO_4$, at a temperature of 80°C and a cathodic current density of 100 ma/cm^2 to build up a hydride surface film. The required charging times were a function of the desired hydride film thickness and are illustrated in Figure 10. Following the cathodic charging, the insulating lacquer was removed and the diffusion couples were inserted into a 600°C tube furnace for twelve minutes in an air environment to allow the hydrogen from the hydride surface film to equilibrate via diffusion through the thickness of the test specimens. The specimens were then air quenched to room temperature. Finally, the outer surfaces were vapor blasted and pickled to remove approximately 50 μm of material per surface prior to final test exposures. Again, two types of diffusion couples were created, one with an initial solid-solution gradient at test temperature and one with only an initial precipitated hydride diffusion gradient at test temperature.

Test Conditions

Applied-Stress Samples

The applied-stress samples of Figure 7, investigating the mechanism of equation 1, were isothermally tested at four temperatures under either applied tensile or compressive stress loadings. The exposure conditions for these samples are summarized in Table 2. Load was applied with levered hanging weights. Temperature was controlled with clamshell furnaces, with an internal air environment.

Temperature was monitored on the test specimens above, below, and in the gage section by thermocouples. At each temperature, specimens uniformly precharged above the stress-free precipitation solvus at the test temperature and specimens uniformly precharged below the stress-free precipitation solvus at the test temperature were tested. The duration of each test exposure was established to allow hydrogen to diffuse into or out of the thick reservoir region of the specimen along the length of the gage section in accordance with the criterion:

$$4Dt/L^2 = 1 \qquad (10)$$

where:

D = the diffusion coefficient of hydrogen through Zircaloy as reported in [1],

t = time, and

L = the gage length of the specimen.

In all cases, the exposure temperatures were held constant with time.

The applied-stress samples of Figure 8, investigating the mechanism of equation 2, were isothermally tested at three temperatures. The exposure conditions for these samples are summarized in Table 3. Again, both tensile and compressive loading were used. The methods of load application and temperature application were the same as for the dog-bone specimens. Only hydrogen precharged levels above the stress-free precipitation solvus were utilized at each temperature. For these specimens, thermal cycling under constant dead-weight loading was made a test variable at each temperature. Each thermal cycle consisted of a hold at the test temperature of sufficient duration for hydrogen to diffuse the length of the gage section as determined by Equation 10, a furnace cool to below ~90°F requiring approximately 2 hrs, and a rapid heat up back to test temperature. All portions of the thermal cycle were performed with the load held constant.

Six plane-strain tensile samples were tested as above, except that a thermal gradient was superimposed upon the stress gradient. The test conditions of these samples also are summarized in

Table 3. The purpose of these samples was to compare directly the relative effects of a thermal gradient and a stress gradient on hydrogen migration. The thermal gradient was imposed by wrapping nicrome wire around the gage length of each specimen and imposing a current through the wire with a DC power supply. The entire assembly was then inserted in a clamshell furnace under dead-weight loading. Temperatures were monitored along the length of the sample with thermocouples as indicated in Figure 11. The temperature profiles imposed on the samples are provided in Table 4. Thermal cycling was performed as summarized above with the DC current being switched off as a part of each thermal cycle. For each of the thermal gradients tested, a control sample was run with no imposed stress gradient.

Self-Stress Samples

The self-stress hydrogen concentration diffusion couples of Figure 9 were isothermally exposed at one test temperature, 360°C. The exposure conditions are summarized in Table 5. Two different hydrogen concentration profiles were used: the first with the hydrogen concentration on both sides of the diffusion couple above the stress-free precipitation solvus at test temperature (~300ppm/~600ppm), the second with the hydrogen concentration on one side above and on the other side below the stress-free precipitation solvus at test temperature (~10ppm/~400ppm). The test specimens were annealed in two groups at 360° C in a furnace containing an air environment. The first group was exposed continuously for 100 days with no thermal cycles. The second was exposed for ten cycles of ten days each. Each cycle consisted of a heatup to 360° C, a ten-day hold, and a slow (furnace) cool to room temperature. The ten-day hold period was established on the basis of a one-dimensional diffusion calculation into a finite plane [45]. If different solid-solution hydrogen concentrations are established on each side of the thermal couple, ten days is the time required for the two sides to come to within 50 percent of equilibrium on the basis of the diffusion coefficient for hydrogen reported in Reference [1].

Measurements After Exposure

Following the test exposures summarized in Tables 2 through 5, all test specimens were destructively analyzed to determine the degree of hydrogen migration that had occurred. Hydrogen concentration measurements were made both qualitatively via light optical metallography, and quantitatively with a LECO hydrogen analyzer. The LECO hydrogen analyzer determined the hydrogen concentration of each test sample by first fusing the alloy in the presence of a tin flux. A nitrogen carrier gas then swept the evolved hydrogen gas into a thermal conductivity cell. The quantity of hydrogen gas evolved was determined by measuring the thermal conductivity of the nitrogen-hydrogen gas mixture and comparing the results obtained with known quantities of hydrogen derived either from National Bureau of Standards (NBS) zirconium standards or an alloquat of hydrogen gas injected into the system. The reported accuracy of the technique is +/- 10 percent of the measured concentration. Repeat analyses of duplicate samples indicated that when comparing concentrations of companion samples analyzed consecutively, the precision of the technique is approximately +/- 5 percent.

To meet the sample size limitations of the LECO technique, and to obtain several analyses along the stress gradients, the test specimens were sectioned as indicated in Figure 12. This sectioning provided both a metallographic sample along the entire length of the possible hydrogen concentration gradient, and several ~0.1g hydrogen-extraction samples along the length of the stress gradients. Hydrogen-extraction samples derived from any single test specimen were sequentially analyzed on the same day, preceded and followed by NBS zirconium standards, to minimize the relative error among measurements from a single test specimen. This minimized errors in inferences regarding the existence of hydrogen concentration gradients in any single test specimen.

The metallographic samples were prepared by first mounting the sample in cross-section in hysol to view the interior edge of the metallographic section. A minimum of 0.76mm of material was ground from the cut surface using sequentially finer grades of silicon carbide paper. The samples were then polished to a mirror finish using a slurry of Linde B diamond paste, and metallographically etched to bring

out the hydrides using a swab etch of 70 cc HNO_3, 30cc H_2O_2, and three drops of HF.

Experimental Results

Dog-Bone-Shaped Applied-Stress Specimens

The gas extraction results for both the tensile and compressive test specimens are tabulated in Table 6. The 316°C data are plotted in Figure 13 as illustrative of results at all temperatures. All specimens are seen to have developed little if any hydrogen concentration gradient along the length of the gage section. The measured hydrogen levels are very uniform (standard deviation of <10ppm) and well within the experimental error of the hydrogen measurement technique. Most specimens exhibit within-specimen hydrogen concentration variations of less than four ppm.

Representative metallography from the 316°C test samples are provided in Figure 14. Two micrographs from the specimen are shown, one in the thinnest region of the neck and the second in the thick reservoir region of the specimen. No evidence was observed in these test specimens, over the entire stress range tested, of either hydride reorientation or redistribution due to either tensile or compressive stress gradients.

Thermally Cycled Applied-Stress Specimens

The gas-extraction results from the tensile-stressed and compressive-stressed thermal-cycled samples are provided in Table 7. Representative post-test hydrogen concentration measurements are illustrated in Figure 15. In this set of test samples, a net transfer of hydrogen is observed to have occurred into the gage section of the tensile specimens and out of the gage section of the compressive samples. The amount of net transfer of hydrogen increased with the exposure temperature, the magnitude of the applied stress, and the number of thermal cycles, as illustrated in Figure 16. The net transfer of hydrogen was determined as the difference between the measured concentration of the reduced gage section and the average of the samples far removed from the gage section. If the difference was within

two sigma of the average concentration of the far removed samples, no net transfer of hydrogen was inferred.

Representative metallography of the isothermal test specimens is illustrated in Figure 17 from the 371°C specimens. Metallography from the gage section and the low-stressed end region are shown. The increase of approximate 200 ppm in the hydrogen concentration of the gage section of the thermally cycled sample is not evident in the metallography. In addition, no evidence for alignment of the hydride perpendicular to the stress axis was observed.

The gas-extraction results from the tensile samples tested in combination with an imposed thermal gradient are provided in Table 8. The representative results from one set of the approximate 28°C delta samples are plotted in Figure 18. A large net transfer of hydrogen out of the gage section is seen to have occurred independent of the applied stress. In addition, the remaining hydrogen concentration in the gage section is independent of the applied stress gradient.

Self-Stress Specimens

The hydrogen gas-extraction results from the self-stressed samples are illustrated in Figures 19 and 20. Figure 19 provides the initial ~300ppm/~600ppm diffusion couple results and Figure 20 provides the initial ~10ppm/~400ppm diffusion couple results. As illustrated in Figure 19, no net transport of hydrogen occurred within the ~300ppm/~600ppm diffusion couple, within the accuracy of the measurement technique, either in the presence or in the absence of thermal cycling. As shown in Figure 20, a net transport of hydrogen did occur from the initial high-concentration side to the initial low-concentration side of the ~10ppm/~400ppm diffusion couples, both in the presence and in the absence of thermal cycling, producing a final uniform hydrogen concentration of approximately ~140 ppm across the initially ~10 ppm end. Both the cycled and noncycled ~10ppm/~400ppm specimens behaved the same within the accuracy of the measurement technique.

Discussion

Dog-Bone Shaped Applied-Stress Specimens

The dog-bone shaped test specimens were specifically designed to create a linear stress gradient along the length of the test specimens. In this way any observed linear gradient in hydrogen concentration along the length of the test specimens directly relates to the linear gradient in the applied stress, as described by equation 9. The results of a linear regression analysis of the hydrogen concentration measurements of Table 6 to the model:

$$[H] = A + Bx \tag{11}$$

where:

[H] = the measured hydrogen concentration , and

x = position along the gage length

are shown in Table 9. The results of the linear regression analysis show little correlation of the measured hydrogen concentration to position along the gage length and therefore to stress. This result shows stress, as described by equation 1, to have little impact within the accuracy of the hydrogen extraction measurements, on the solid solution-hydrogen concentration profile.

Thermally Cycled Applied-Stress Specimens

The thermally cycled plane-strain tensile specimens and the thermally cycled uniaxial compression specimens show that a combination of thermal cycling and an applied stress gradient produces a net transfer of hydrogen in an isothermal specimen (Figure 16). The amount of the net transfer is a function of the test temperature, applied stress, and number of thermal cycles. The observations are consistent with a small amount of hydrogen being delivered into or out of the gage section with each thermal cycle, and for the net transfer being proportional to the number of thermal cycles (a ratcheting effect). The observed net transfer per cycle occurring under each test condition is summarized in Table 10. Because the cooldown periods of the thermally cycled specimens and the hold

times at the cold temperature were too short for long-range diffusion into or out of the gage length to have occurred, the measured transfer must have occurred during the high temperature anneals. This means the condition causing the transfer must have been established either during the heat-up, or during the high temperature thermal anneal itself.

The thermal cycle experiments, as conducted, can not unambiguously differentiate between equations (1) and (2) as potential mechanisms resulting in the net transfer of hydrogen into or out of the gage sections. The experimental results can be explained in terms of Equation 2 by relating the amount of hydrogen dissolving from the hydrides into solid solution, during heat up, as a decreasing function of applied tensile stress. This creates a solid solution concentration gradient in the sample, and solid-solution diffusion of hydrogen would then occur during the high-temperature hold periods until the solid solution concentration of hydrogen in the gage section is in equilibrium with the low-stressed region of the specimen. The net transfer of hydrogen would stop at this point due to the significant supersaturation of the Zircaloy matrix required for hydride precipitation [*1*]. The cooldown cycle would precipitate out the majority of hydrogen in solid solution (freezing it in place), and transfer of hydrogen would begin again with the next heat-up in the test sequence. The net transfer per cycle inferred from the test data of Figure 16 and tabulated in Table 10 is then a measure of the effect of the applied stress on the hydride dissolution solvus in Zircaloy. A least square linear regression analysis of equation 2 to the data of Table 10 gives the following equation for the effect of stress on the hydride dissolution solvus:

$$C = C_o \exp(-1.8\sigma_H/RT) \qquad (11)$$

where:

σ_H = the hydrostatic stress in MPa,

R = the gas constant in joules/mole-°K,

T = temperature in degrees kelvin.

And the quantity $(V - V_H)$ in equation 2 has the value -1.8×10^{-6} m^3/mole.

This interpretation of the data is also consistent with the thermal gradient data summarized in Table 8 and illustrated in Figure 18. With the formulation of Equation 11, the effect of stress on the hydride dissolution solvus is much smaller than the effect of temperature on the dissolution solvus, as illustrated on Figure 21. Temperature gradients within a Zircaloy-hydride two-phase field would therefore be expected to produce much larger solid-solution gradients than do applied stress gradients, and therefore should have a much larger effect on hydrogen migration. This is what was observed in the thermal gradient experiments.

This interpretation of the data is however inconsistent with independent measurements in the literature for V and V_H. MacEwen et.al. [46] used time of flight neutron diffraction to measure the dilation of the zirconium lattice by interstitial deuterium and concluded V was 1.67×10^{-6} m^3mole. From the work of Carpenter [47], a value of 1.45×10^{-6} m^3/mole has been estimated for V_H [27]. With these two values, the difference $V - V_H$ is approximately an order of magnitude smaller than the quantity in Equation 11 above, suggesting any stress effect of the hydrogen solvus is too small to explain the experimental observations reported here in.

It is also possible that the experimental observations reported here in as a result of the "ratcheting" of the effect of a stress gradient on hydrogen diffusion as described by equation 1. The effect may not have been observed in the dog-bone shaped specimens because without thermal cycling it is too small to be identified within the accuracy of the experimental measurements. Fitting equation 1 to the thermal cycle data a value of 1.8×10^{-6} m^3/mole is obtained for V. This value is in good agreement with measurement of MacEwen [46] of 1.67×10^{-6} m^3/mole and with the microcalorimtry measurements of Eadie et.al. [35] which inferred a value of 1.87×10^{-6} m^3/mole for V.

To unambiguously determine whether the net transfer of hydrogen observed in the subject experiments is a result of a stress effect on the dissolution solvus or a stress effect on the chemical potential of hydrogen dissolved in solid solution, the thermal cycle experiments need to be repeated, this time only applying load during the high temperature anneal and removing it

during the heat up and cool down periods. If the applied stress is only impacting the dissolution solvus, no net transfer of hydrogen will occur under this loading condition.

Self-Stressed Samples

The experimental results from the ~300ppm/~600ppm hydrogen diffusion couples are in agreement with the hydrogen solvus model described in Reference [1] and summarized in Table 1. The results show that the hydrogen concentration dissolved in the Zircaloy matrix is independent of the total hydride concentration of the region, and therefore k_s in equation 5 is equal to zero. With k_s equal to zero, both sides of the ~300/~600ppm diffusional couple achieve the same solid-solution concentration at test temperature and no solid-solution concentration gradient exists to drive hydrogen migration from one side of the specimen to the other.

A net transport of hydrogen is observed in the ~10ppm/~400ppm diffusion couples from the initial high-concentration side to the initial low-concentration side. This is expected based on the solid-solution concentration gradient established in these specimens. At the beginning of test, enough of the hydride dissolves on the initial ~400 ppm side to put approximately 140 ppm into solid solution in the matrix. Only 10 ppm is available on the initial 10 ppm side and therefore a large solid-solution gradient exists at the start of the specimen exposure. Hydrogen diffuses from the high-concentration end to the low-concentration end until the two solid-solution concentrations are identical and no solid-solution concentration gradient exists. The excess hydride on the high-concentration end continues to supply hydrogen to the high-concentration end matrix during the diffusion process to maintain it near the 140 ppm level. A solvus concentration of 140 ppm at a temperature of 360°C is in good agreement with the hydride dissolution solvus measurements of Reference [1].

The final hydrogen concentration profiles on the initially high-concentration end of the ~10ppm/~400ppm diffusion couples, however, are not in agreement with the diffusion model of Reference [1]. The calculated post-anneal profile using that model is illustrated in Figure 22, along with the pre-test

and post-test measurements. The model predicts that the hydrogen will be supplied to the initial low-concentration region only from the interface of the hydride bearing region, and that regions deeper into the high-concentration end would not know a solid-solution concentration gradient exists anywhere in the sample. This is because the model of Reference [1] asumes that hydride dissolution to supply the matrix with hydrogen is essentially instantaneous [48], allowing no solid-solution concentration gradient to develop across an isothermal two-phase region. During an isothermal anneal, this would cause the interface between the hydride-containing region and the nonhydride-containing region at temperature to move essentially as a propagating wave. The experimental measurements suggest that diffusion of hydrogen occurred out of the entire initially high-hydrogen side, even though the entire region was two phase at temperature. These experimental results suggest that hydride dissolution may be more sluggish than modeled, allowing some solid-solution concentration gradient to be established across the entire two-phase region even under isothermal conditions.

Conclusions

1) An applied stress gradient through a Zircaloy component resulted in a non-detectable transfer of hydrogen into or out of the stressed region in the absence of thermal cycling. This demonstrates that any effect of stress either on the chemical potential of hydrogen in solid solution or on the hydrogen solvus is small.

2) An applied stress gradient on a Zircaloy component can produce a measurable and nonnegligeable net transfer of hydrogen into or out of a hydride containing region in the presence of thermal cycling. Hydrogen migrates into high tensile regions and out of high compression regions Thermal cycling is likely required to accentuate the observed hydrogen transport occurring during the high-temperature hold periods due to the hysterisis on the hydride dissolution and precipitation solvus in Zircaloy.

3) The experimental results reported herein of hydrogen transport occurring during the high-temperature hold periods of the thermal cycles are consistent with a stress effect on the hydride dissolution solvus as described by Equation 2:

$$C = C_o \exp((V - V_H)\,\sigma_H/RT))$$

where $(V - V_H)$ has the value -1.8×10^{-6} m^3/mole. Independent measurements in the literature for V and V_H, however, suggest their difference is an order of magnitude smaller.

4) The observed net transfer of hydrogen under thermal cycle conditions is also consistent with a stress effect on the chemical potential of hydrogen dissolved in solid solution where V has the value of 1.8×10^{-6} m^3 mole. This value of V is consistent with other measurements in the literature.

5) The experiments described here-in can not unambiguously assign the cause of the observed net transfer of hydrogen to either an effect of stress on the dissolution solvus or to an effect of stress on the chemical potential of hydrogen dissolved in the Zircaloy lattice. To do this, the experiments must be repeated to remove the applied stress during the heat-up and cool-down periods.

6) The hydride dissolution solvus is independent of the hydride concentration of a two-phase alpha plus delta hydride region up to the hydrogen concentration levels investigated, i.e., up to approximately 1000 ppm hydrogen.

7) Any effect of an applied stress on hydrogen migration is small compared to the effect of temperature. Any power-produced temperature gradients existing within a component will likely override the small effect of stress on the long-range migration of hydrogen.

8) The dissolution of a hydride to supply the surrounding matrix with hydrogen is more sluggish than

assumed in the diffusion model of Reference [1]. The more sluggish kinetics allow a solid-solution concentration gradient to develop across a two-phase field even under isothermal conditions.

Acknowledgments

The authors of this paper gratefully acknowledge the work of other Bettis staff in support of the reported experiments. Mr. K.B. Marsh and Mr. P. F. Thompson carefully hydrogen precharged the test specimens; Mr. E. R. Ferchak. Mr. V. R. Wiederkehr, and Dr. L.G. Irr accurately measured the hydrogen concentration of hundreds of samples in a timely manner; and Ms. M. A. Kenny carefully typed and edited the manuscript. Dr. A. N. Lord of the Knolls Atomic Power Laboratory is acknowledged for developing the self-stress solubility model. Finally, the review comments of the ASTM symposia participants, particularly Dr. C. E. Ells, formally of AECL, are gratefully acknowledged.

References

1. Kammenzind, B. F., et al., "Hydrogen Pickup and Redistribution in Alpha Annealed Zircaloy-4", Zirconium in the Nuclear Industry: Eleventh International Symposium, ASTM STP 1295, 1996, pp. 338-370.

2. Clayton, J. C., "Out-of-Pile Nickel Alloy-Induced Accelerated Hydriding of Zircaloy Fasteners", Zirconium in the Nuclear Industry: Sixth International Symposium, ASTM STP 824, 1984, pp. 572-591.

3. Clayton, J. C., "Internal Hydriding in Irradiated Defected Zircaloy Fuel Rods", Zirconium in the Nuclear Industry: Eighth International Symposium, ASTM-STP 1023, 1988, pp. 266-288.

4. Someno, M., "Determination of the Solubility and Diffusion Coefficient of Hydrogen in Zirconium", Nihon Kinzoku Gakkaishi, Vol. 24, 1960, pp. 249-253.

5. Sawatzky, A., "The Diffusion and Solubility of Hydrogen in the Alpha Phase of Zircaloy-2, "Journal of Nuclear Materials, Vol. 2 1960, pp. 62-68.

6. Mallet, M. W. and Albrecht, W. M., "Low Pressure Solubility and Diffusion of Hydrogen in Zirconium", Journal of the Electrochemical Society, Vol. 104, 1957, pp. 142.

7. Slattery, G. F., "The Terminal Solubility of Hydrogen in Zirconium Alloys between 30 and 400°C", Journal of the Institute of Metals, Vol. 95, 1967, pp. 43-47.

8. Kearns, J. J., "Terminal Solubility and Partitioning of Hydrogen in the Alpha Phase of Zirconium, Zircaloy-2 and Zircaloy-4", Journal of Nuclear Materials, Vol. 22, 1967, pp. 292-303.

9. Erickson, W. H. And Hardie, D., "The Influence of Alloying Elements on the Terminal Solubility of Hydrogen in a Zirconium", Journal of Nuclear Materials, Vol. 13, 1964, pp. 254-262.

10. Sawatzky, A. and Wilkins, B. J. S., "Hydrogen Solubility in Zirconium Alloys Determined by Thermal Diffusion", Journal of Nuclear Materials, Vol. 22, 1967, pp. 304-310.

11. Kreyns, P.H., et al., "Embrittlement of Reactor Core Materials", Zirconium in the Nuclear Industry: Eleventh International Symposium, ASTM STP 1295, 1996, pp. 758-782.

12. Grigoriev, V., et al., "Fracture Toughness of Zircaloy Cladding Tubes", Zirconium in the Nuclear Industry: Eleventh International Symposium, ASTM STP 1295, 1996, pp. 431-447.

13. Garde, A.M., et al., "Effects of Hydride Precipitate Localization and Neutron Fluence on the Ductility of Irradiated Zircaloy-4", Zirconium in the Nuclear Industry: Eleventh International Symposium, ASTM STP 1295, 1996, pp. 407-430.

14. Kearns, J. J., et al, "Effect of Texture, Grain Size, and Cold Work on the Precipitating of Oriented Hydrides in Zircaloy Tubing and Plate", Journal of Nuclear Materials, Vol. 20, 1966, pp. 241-261.

15. Blat, Martine, Noel, Didier, "Detrimental Role of Hydrogen on the Corrosion Rate of Zirconium Alloys", Zirconium in the Nuclear Industry: Eleventh International Symposium, ASTM STP 1295,

1996, pp. 319-337.

16. Knights, C. F., and Perkins, R., "The Effect of Applied Tensile Stress on the Corrosion Behavior of Zircaloy-2 in Steam and Oxygen", Journal of Nuclear Materials, Vol. 36, 1970, pp. 180-188.

17. Kim, Young Suk, et al., "Effect of Hoop Stress on Corrosion of Zircaloy-4 Cladding Tube", Journal of Nuclear Materials, Vol. 223, 1995, pp. 163-168.

18. Garde, A. M., "Enhancement of Aqueous Corrosion of Zircaloy-4 Due to Hydride Precipitation at the Metal Oxide Interface", Zirconium in the Nuclear Industry: Ninth International Symposium, ASTM-STP 1132, 1991, pp. 566-594.

19. Cheng, B., "PWR Zircaloy Fuel Cladding Corrosion Performance, Mechanisms, and Modeling", Zirconium in the Nuclear Industry: Eleventh International Symposium, ASTM STP 1295, 1996, pp. 137-160.

20. Cupp, C. R., Flubacher, P., "An Autioradiographic Technique For the Study of Tritium in Metals and its Application to Diffusion in Zirconium at 149 C to 240 C", Journal of Nuclear Materials, Vol. 6, No. 2, 1962, pp. 213-228.

21. Mazzolai, M., Ryll-Nardzewski, J., "An Anelastic Study of the Diffusion Coefficient of Hydrogen in α-Zirconium", Journal of the Less Common Metals, Vol. 49, 1976, pp. 323-327.

22. Kearns, J. J., "Diffusion Coefficient of Hydrogen in Alpha Zirconium, Zircaloy-2, and Zircaloy-4", Journal of Nuclear Materials, Vol. 43, 1972, pp. 330-338.

23. Marino, G. P., "HYDIZ-A 2-Dimensional Computer Program for Migration of Interstitial Solutes of Finite Solubility in a Thermal Gradient", WAPD-TM-1157, National Technical Information Service, Springfield, VA, June 1974.

24. Li, J.C.M., Oriani, R. A., and Darken, "The Thermodynamics of Stressed Solids", L. S. Z Phys. Chem. Nev. Folge., Vol. 49, pp. 271-291, 1966, pp. 271-290.

25. Puls, M. P. "The Effect of Misfit and External Stresses on Terminal Solid Solubility in Hydride-Forming Metals", Acta Met, Vol, 29, 1981, pp. 1961-1968.

26. Puls, M. P., "Elastic and Plastic Accommodation Effects on Metal-Hydride solubility", Acta Met, Vol, 32, 1984, pp. 1259-1269.

27. Coleman, C. E., Amber, J. F. R., "Solubility of Hydrogen Isotopes in Stressed Hydride Forming Metals", Scripta Metallurgical, Vol. 17, 1983, pp. 77-82.

28. Eshelby, J. D., "The Determination of the Elastic Field of an Ellipsordial Inclusion, and Related Problems", Proc. R. Soc, A241, 376, 1957.

29. Eshelby, J. D., "the Continuing Theory of Lattic Defects", Solid State Physics, Vol. 3, Academic Press, 1956, pp. 79.

30. Markowitz, J. M., "Hydrogen Redistribution in Zircaloy-2 Under Thermal and Mechanical Stress Gradients", WAPD-TM-171, dated January 1959.

31. Ells, C. E., Simpson, C. J., "Stress Induced Movements of Hydrogen in Zirconium Alloys", Hydrogen in Metals (edited by I. M. Bernstein and A. W. Thompson), Am Soc. Metals, 1974, pp. 345.

32. Stevens, R. N., Dutton, R., "The Effect of Temperature Pressure, and Concentration Gradients on Diffusion", Atomic Energy of Canada Limited Report, AECL-3793, 1971.

33. Dutton, R., Puls, M. P., "A Theoretical Model for Hydrogen Induced Sub-Critical Crack Growth", Effect of Hydrogen on the Behavior of Materials, AIME, 1976, pp. 428-440.

34. Eadie, R. L., Coleman, C. E., "Effects of Stress on Hydride Precipitation in Zirconium-2.5% Niobium and on Delayed Hydride Cracking", Scripta Metallurgical, Vol. 23, 1989, pp. 1865-1870.

35. Eadie, R. L., Tashio, K., Harrington, D., Leger M., "The Determination of the Partial Molar Volume of Hydrogen in Zirconium in A Simple Stress Gradient Using Comparative Micro calorimetry", Scripta Metallurgical, Vol. 26, 1992, pp. 231-236.

36. Parry, G. W., "Strain Induced Directionality of Zirconium Hydride Precipitates in Zirconium-2.5 w/o Nb - 0.5 w/o Cu Alloy", Atomic Energy of Canada Limited Report, AECL-1888, 1963.

37 Louthan, M. R., Angerman, C. L., "Thermomechanical Effects on Hydride Precipitation in Zircaloy-2", Met Trans 1973, Vol. 4, pp. 1763-1765.

38. Mishima, Y., et al., "Effect of Thermal Cycling on the Stress Orientation of Hydrides in Zircaloy", Met Trans 1971, Vol. 2, 1995.

39. Mishima, Y., Okubo, T., "Effect of Thermal Cycling on the Stress Orientation and Circumferential Ductility in Zircaloy-2", Can Met Quart, 1972, Vol. 11, pp. 157-164.

40. Charquet, D. et al., "Influence of Variations in Early Fabrication Steps on Corrosion, Mechanical Properties, and Structure of Zircaloy-4 Products", Zirconium in the Nuclear Industry: Seventh International Symposium, ASTM STP 939, 1987, pp. 431-447.

41. Foster, J. P., "Influence of Final Recrystallization Heat Treatment on Zircaloy-4 Strip Corrosion", Journal of Nuclear Materials, Vol. 173, 1990, pgs. 164-178.

42. Rudling, P., et al., "Corrosion Performance of Zircaloy-2 and Zircaloy-4 PWR Fuel Cladding", Zirconium in the Nuclear Industry: Eighth International Symposium, ASTM STP 1023, 1989, pp. 213.

43. Kearns, J. J., "Laboratory Method for Adjusting Hydrogen Content of Zirconium", WAPD-TM-147, 1958.

44. Sawatzky, A., "Hydriding Zircaloy-2 by Electrolysis", AECL Report #1046, 1960.

45. Crank, J., Mathematics of Diffusion, Oxford, 1956.

46. MacEwen, S. R., Coleman, C. E., Ells, C. E. And Faber, J., "Dilation of hcp Zirconium by Interstitial Deuterium", Acta Met, Vol. 33, 1985, pp. 753-757.

47. Carpenter, G.J.C., "The Dilational Misfit of Zirconium Hydrides Precipitated in Zirconium", Journal of Nuclear Materials, Vol. 48, 1973, pp. 264-266.

48. Kearns, J. J., "Dissolution Kinetics of Hydride Platelet in Zircaloy-4", Journal of Nuclear Materials, Vol. 27, 1968 pps. 64-72.

Table 1

Model Used for the Migration of Hydrogen

I. Hydrogen diffuses through the alpha (hcp) phase in response to temperature and solid solution concentration gradients.

$$\vec{J} = D\vec{\nabla}C - \frac{DQ^*C}{RT^2}\vec{\nabla}T$$

where

J = the flux of diffusing atoms,
D = diffusion coefficient of hydrogen through Zircaloy,
C = solid solution concentration of hydrogen in Zircaloy,
Q* = heat of transport,
T = temperature, and
R = the gas constant.

The rate of change in hydrogen concentration at a point is

$$\frac{\delta C_T}{\delta t} = -\vec{\nabla}\cdot\vec{J}$$

and the rate of change of hydrogen in solid solution in the α Zircaloy is

$$\frac{\delta C}{\delta t} = -\vec{\nabla}\cdot\vec{J} - \alpha^2(C - C_{PT}), \qquad \text{If } C > C_{PT}$$

$$\frac{\delta C}{\delta t} = -\vec{\nabla}\cdot\vec{J}, \qquad \text{If } C_{eq} < C < C_{PT}$$

$$\frac{\delta C}{\delta t} = 0, \qquad \text{If } C=C_{eq} \text{ and hydrides are present}$$

where

C_T = total hydrogen concentration,
C_{PT} = C_{PTO} exp (-Q_P/RT), concentration for precipitation,
C_{eq} = C_{eqo} exp (-Q_{eq}/RT), concentration for dissolution, and
α^2 = α_o^2 exp (-2 Q_f/RT), fitted rate parameter for precipitation.

Table 2

Exposure Conditions of Conical Applied Stress Samples

	TEMPERATURE (C)	HYDROGEN PRECHARGING* (PPM)	EXPOSURE TIME*** (DAYS)	MAXIMUM STRESS** (MPa)	STRESS GRADIENT (MPa/CM)
1.	260	30	60	172	121
2.	260	90	60	172	121
3.	316	60	25	172	121
4.	316	140	25	172	121
5.	371	120	11	145	101
6.	371	210	11	145	101
7.	427	200	6	110	77
8.	427	310	6	110	77

* One hydrogen level is significantly (~25%) below the solubility limit, the other ~50 ppm above the solubility limit.

** This maximum stress is based upon limiting tensile creep of the thinnest region to <5% at the given exposure time. Each experiment was performed on both the tensile and compressive specimens.

*** This exposure time is the time required for hydrogen to come to equilibrium by diffusion across the gage length.

Table 3

Exposure Conditions of
Thermal-Cycled, Applied-Stress Test Specimens

Anneal Temperature (°C)	Stress (MPa)	Anneal Duration		
		Constant Temp.	Thermally Cycled	
260	160	None	None	25 cycles, 4 days each
260	240	100 days	10 cycles, 4 days each	None
315	160	100 days	10 cycles, 4 days each	None
315	240	100 days	10 cycles, 4 days each	25 cycles, 4 days each
371	160	None	10 cycles, 2 days each	25 cycles, 2 days each
371	240	50 days	10 cycles, 2 days each	25 cycles, 2 days each
371	-138	None	None	25 cycles, 2 days each
371	-159	None	None	25 cycles, 2 days each
315 gage 260 shoulder	240	None	10 cycles, 10 days each	None
315 gage 288 shoulder	310	None	10 cycles, 10 days each	None
371 gage 343 shoulder	310	None	None	25 cycles, 2 days each

Table 4

Temperature Profiles of Thermal Gradient Samples (°C)

Position/(cm)	OTT 010	OTT 020	TS 26	TS 27	TS 28	TS 29
0.0	312	313	313	316	372	372
0.25	278	269	293	295	353	355
-0.25	278	272	294	297	353	355
0.63	267	264	290	292	351	351
-0.63	265	264	290	292	351	351
1.02	256	253	281	286	343	342
-1.02	256	254	283	288	344	343
2.79	238	234	270	277	332	330
-2.79	239	236	270	278	332	329

Table 5

Exposure Conditions of Self-Stressed Samples

Anneal Temperataure	Concentration Profile (ppm)	Anneal Cycled	
		Constant Temperature	Thermally Cycled
360°C	10/400	100 days	10 cycles of 10 days each
360°C	300/600	100 days	10 cycles of 10 days each

Table 6

Post-Test Hydrogen Extraction Measurements of Dog-Bone Specimens
Tensile Specimens

1. Temperature (C)	427	427	371	371	316	316	260	260
2. Time (day)	6	6	11	11	25	25	60	60
3. Axial Location**	Hydrogen Concentration (ppm)							
0.0 cm (centerline)	271	204	199	116	124	54	75	27
+0.32 cm	271	208	203	110	131	53	76	25
- 0.32 cm	268	203	202	113	129	54	80	25
+0.60 cm	280	201	207	111	130	56	86	26
- 0.60 cm	290	202	206	107	129	55	78	26.
+0.84 cm	292	199	209	109	134	58	77	24
- 0.84 cm	288	201	212	112	130	55	85	21*
+1.12 cm	287	202	210	112	134	53	80	26*
- 1.12 cm	285	199	203	111	132	N/A	84	27
+1.85 cm	281	202	208	108	133	55	80	20*
- 1.85 cm	299	207	213	110	131	55	78	18*
4. Average Post-Test Hydrogen Level and Its Standard Deviation	283±9.3	203±2.9	207±4.2	113±2.0	131±2.7	55±1.4	80±3.5	26±1

* Data suspect. Did not gas extract properly.

** These axial positions are relative to the centerline (thinnest cross section of the specimen). Locations at ± x are the same cross-sectional area.

Table 6 (Continued)

Post -Test Hydrogen Extraction Measurements of Dog-Bone Specimens
Compression Samples

1. Temperature (C)	427	427	371*	315	315	260	260
2. Time (day)	6	6	11	25	25	60	60
3. Axial Location	Hydrogen Concentration (ppm)						
0.0 cm (centerline)	295	199	112	129	55	81	25
+0.32 cm	299	192	112	128	57	84	24
- 0.32 cm	300	201	113	128	51	83	23
+0.60 cm	302	200	118	131	54	80	25
- 0.60 cm	292	195	113	133	54	84	24
+0.84 cm	299	190	114	130	54	84	24
- 0.84 cm	297	192	112	137	53	85	24
+1.12 cm	294	192	113	133	53	83	22
- 1.12 cm	300	195	114	124	56	81	24
+1.85 cm	299	197	111	129	54	81	24
- 1.85 cm	306	188	110	128	60	84	25
4. Average Post-Test Hydrogen Level and Its Standard Deviation	298±3.9	195±4.2	113±2.0	130±3.3	54±1.9	83±1.6	24±0.9

*The 371°C, ~200 ppm run resulted in failure (specimen bending).

Table 7

Post Exposure Hydrogen Gas Extraction Measurements Stressed and Thermally Cycled Samples (ppm)

Position (cm)	260°C 160 MPa (25 Cycles)	260°C 240 MPa (1 Cycle)	260°C 240 MPa (10 Cycles)
0	250	268	232
0.20	223	244	194
-0.20	223	242	213
0.30	260	235	217
-0.30	212	257	202
0.76	--	--	--
-0.76	--	--	--
1.02	248	258	246
-1.02	249	245	212
1.27	--	--	--
-1.27	--	--	--

Table 7 (Continued)

Post Exposure Hydrogen Gas Extraction Measurements Stressed and Thermally Cylced Samples (ppm)

Position (cm)	316°C 160 MPa (1 Cycle)	316°C 160 MPa (10 Cycles)	316°C 240 MPa (1 Cycle)	316°C 240 MPa (10 Cycles)	316°C 240 MPa (25 Cycles)
0	340	338	318	372	404
0.20	332	325	336	356	347
-0.20	348	322	340	345	350
0.30	338	317	344	337	324
-0.30	362	321	344	339	322
0.76	--	--	341	--	356
-0.76	--	--	346	--	339
1.02	346	328	--	359	--
-1.02	362	310	--	344	--
1.27	--	--	337	--	333
-1.27	--	--	347	--	328

Table 7 (Continued)

Post Exposure Hydrogen Gas Extraction Measurements Stressed and Thermally Cycled Samples (ppm)

Position/(cm)	371°C 160 MPa (10 Cycles)	371°C 160 MPa (25 Cycles)	371°C 240 MPa (1 Cycle)	371°C 240 MPa (10 Cycles)	371°C 240 MPa (25 Cycles)
0	330	381	327	402	500
0.20	337	339	345	372	355
-0.20	328	321	335	353	408
0.30	322	320	343	327	308
-0.30	340	319	342	300	308
0.76	--	329	333	--	313
-0.76	--	321	357	--	329
1.02	352	--	--	325	--
-1.02	343	--	--	335	--
1.27	--	337	352	--	319
-1.27	--	349	336	--	325

Table 7 (Continued)

Post Exposure Hydrogen Gas Extraction Measurements Stressed and Thermally Cycled Samples (ppm)

Position/(cm)	371°C -138 Mpa 25 cycles	371°F -159 MPa 25 cylces
0	260	330
0.38	350	340
-0.38	400	370
0.53	400	400
-0.53	390	490
0.84	390	390
-0.84	380	390
1.19	400	410
-1.19	390	--

* Sample buckled during test.

Table 8

Final Hydrogen Concentration Profile (ppm) of Thermal Gradient Samples

Position (cm)	OTT 010 (unstressed)	OTT 020 (310 MPa)	TS 26 (unstressed)	TS 27 (310 MPa)	TS 28 (unstressed)	TS 29 (240 MPa)
0.0	26	30	46	46	110	100
0.15	56	51	50	55	110	100
-0.15	43	48	49	53	100	90
0.23	107	89	55	83	120	100
-0.23	88	74	60	77	120	110
0.48	333	323	120	150	100	110
-0.48	324	320	140	140	130	100
0.79	402	375	180	160	170	150
-0.79	413	382	180	160	180	150
1.19	361	370	200	180	230	280
-1.19	372	362	210	180	240	280
2.79	343	329	190	180	270	300
-2.79	337	321	190	180	270	280

Table 9

Linear Regression Analysis of Dog-Bone Applied-Stress Samples

	Temperature (C)	Hydrogen Precharge (ppm)	Type of Specimen**	A (ppm)*	B (ppm cm^{-1})*	K****	$\frac{\Delta C}{\Delta \sigma}\left(\frac{ppm}{MPa}\right)^{***}$
1.	427	283	T	273.5	+10.9	0.67	14.1×10^{-2}
2.	427	203	T	202.8	- 0.3	- 0.056	0.4×10^{-2}
3.	427	298	C	296.1	+ 2.8	0.43	3.6×10^{-2}
4.	427	195	C	197.5	- 3.3	-0.47	-4.3×10^{-2}
5.	371	207	T	202.1	+ 5.2	0.70	5.1×10^{-2}
6.	371	113	T	112.6	- 2.1	-0.50	-2.1×10^{-2}
7.	371	113	C	114.0	- 1.3	-0.37	-1.3×10^{-2}
8.	315	131	T	128.0	+ 3.0	0.64	2.5×10^{-2}
9.	315	54	T	54.4	+ 0.5	0.19	0.4×10^{-2}
10.	315	130	C	130.5	- 0.6	-0.09	-0.5×10^{-2}
11.	315	54	C	53.3	+ 1.5	0.38	1.2×10^{-2}
12.	260	80	T	78.8	+ 1.2	0.20	1.0×10^{-2}
13.	260	26	T	25.8	+ 0.3	0.11	0.2×10^{-2}
14.	260	83	C	82.7	+ 0.0	0.01	0.0×10^{-2}
15.	260	24	C	24.3	- 0.2	-0.14	-0.2×10^{-2}

* This gas extraction data was fit to the form: [H] = A + Bx, where [H] is the measured hydrogen (ppm), and x is the absolute distance from the thinnest region in the next of the specimen to the point of interest (cm).

** T = tension, C = compression.

*** This was calculated by dividing B, as determined by regression analysis, by , the linear stress gradient.

**** y is the correlation coefficient and represents the goodness-of-fit.

Table 10

Summary of Net Hydrogen Transfer Occurring
in Stressed and Thermally Cycled Test Specimens

Temperature (°C)	Stress (MPa)	Cycles	Net Transfer (ppm)	Net Transfer/Cycle (ppm)
260	160	25	0	0
	241	10	0	0
316	160	10	19	1.9
	241	10	27	2.7
	241	25	65	2.6
371	160	10	0	0
	160	25	47	1.9
	241	10	72	7.2
	241	25	179	7.2
371	-138	25	-130	-5.2
	-159*	25	-70	-2.8

* Sample buckled during test.

Figure 1

Typical Microstructure of Zircaloy-4 Test Material as Revealed by Optical Metallography .

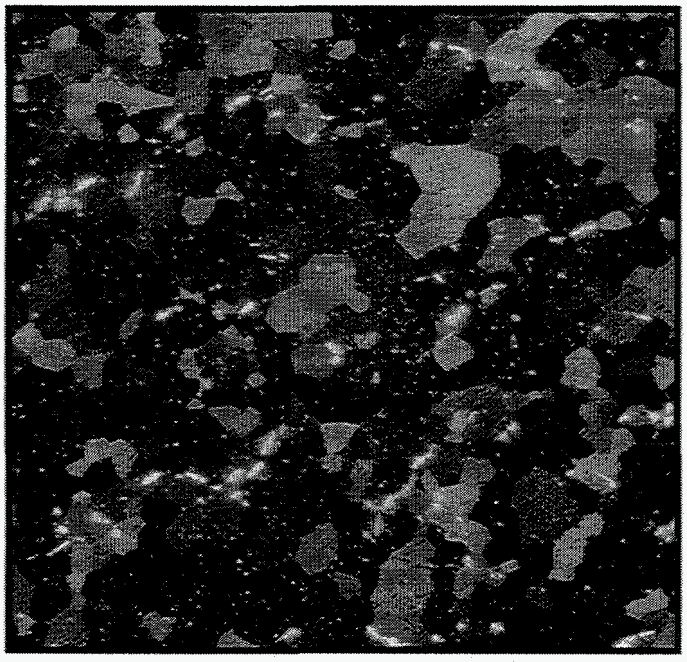

250 X

Transverse to Rolling Direction

Polarized Lighting

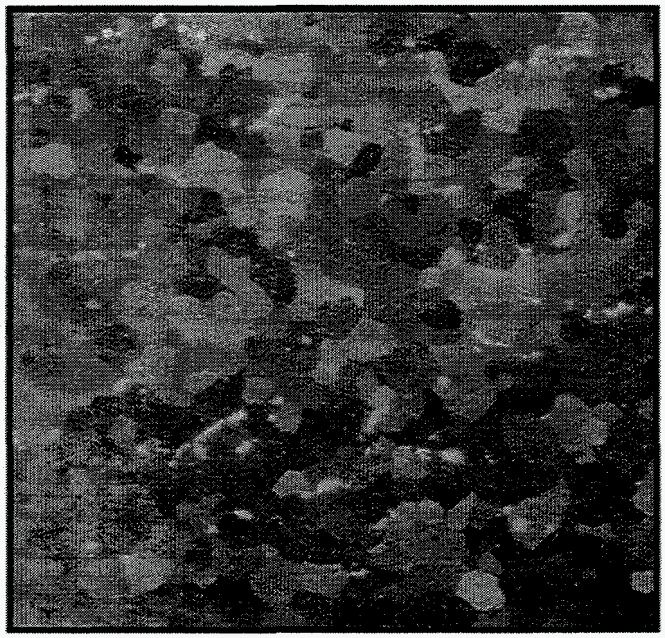

250 X

Rolling Direction

Polarized Lighting

Figure 2

Typical Microstructure of Zircaloy-4 Test Material as Revealed by TEM .

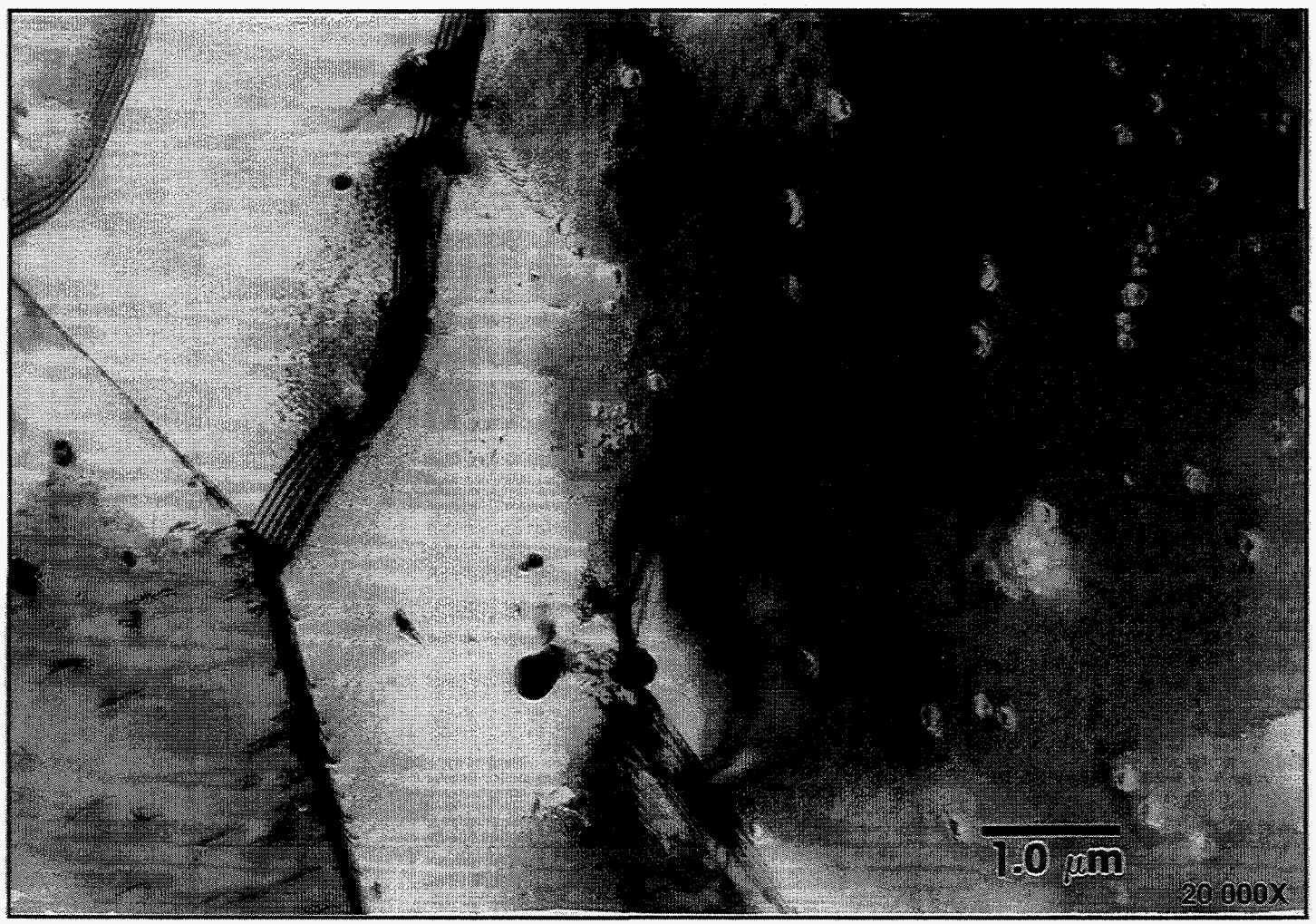

Figure 3

Typical Microstructure of Zircaloy-4 Test Material as Revealed by SEM

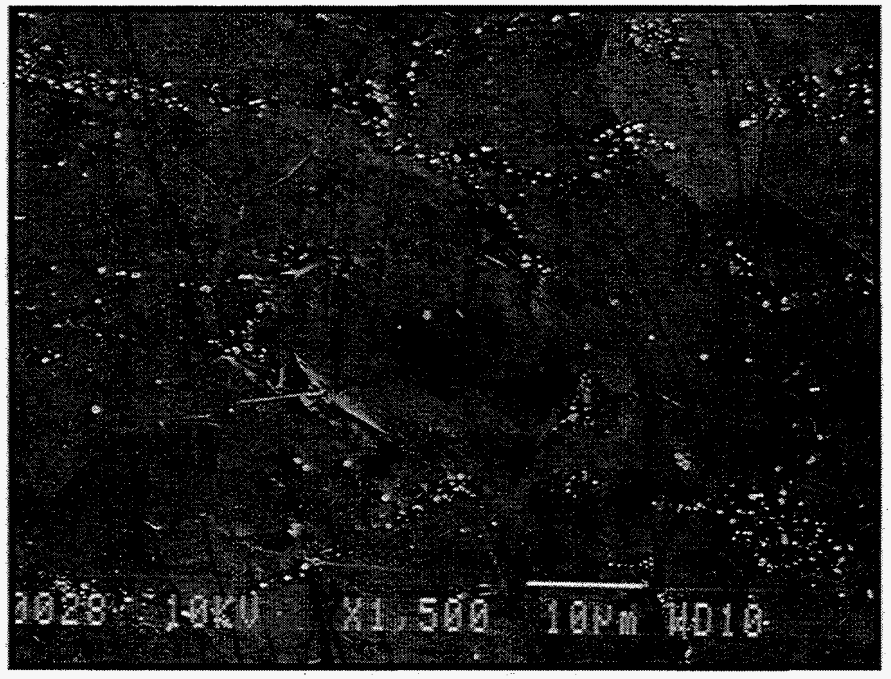

SEM Micrograph with Material Etched to Reveal Precipitates

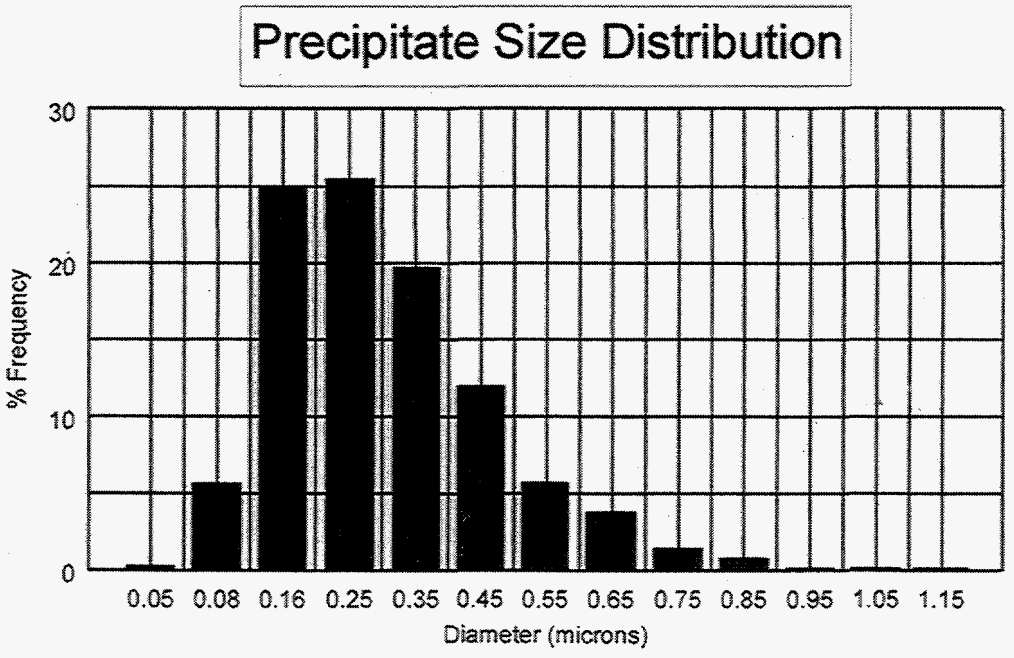

Figure 4

Typical Texture of Test Materials
X-ray Diffraction Inverse Pole Figures

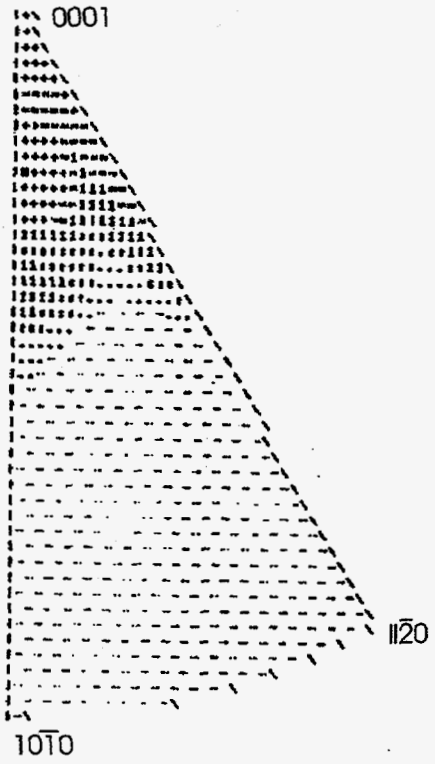

Normal to Rolling Plane
F = 0.724

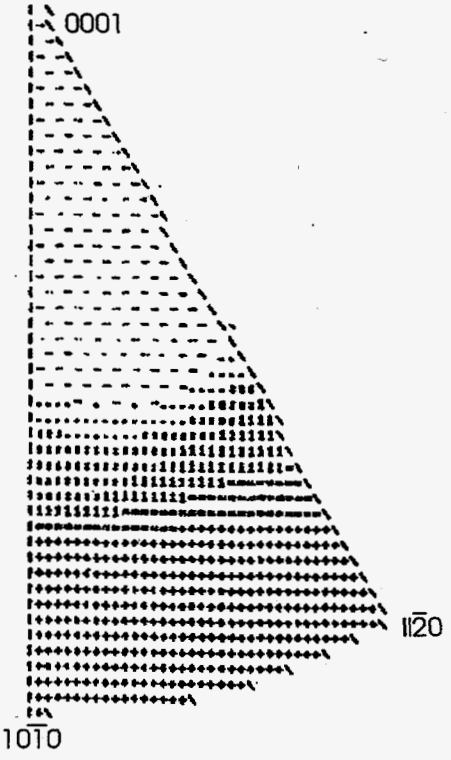

Parallel to Rolling Direction
F = .069

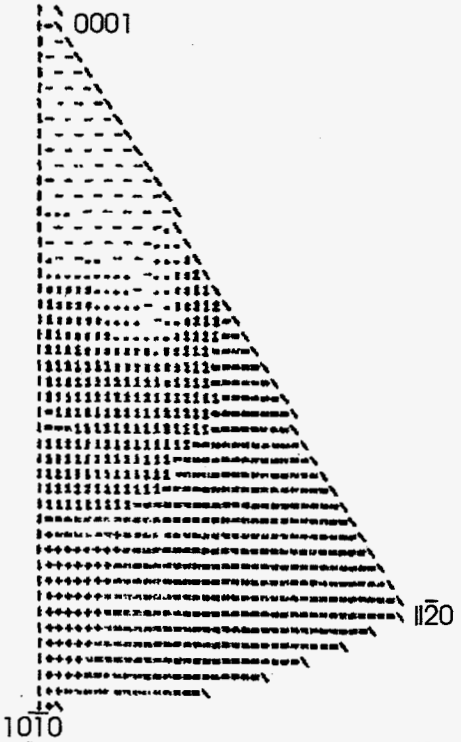

Transverse to Rolling Direction
F = .207

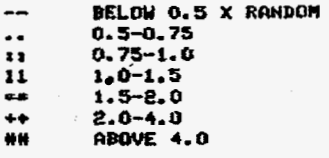

F = No's are average of four separate measurements. Values normalized to 1.

Figure 5

Typical Texture of Zircaloy-4 Test Material Orientation Imaging Microscopy Direct Pole Figures Taken Normal to the Rolling Plane

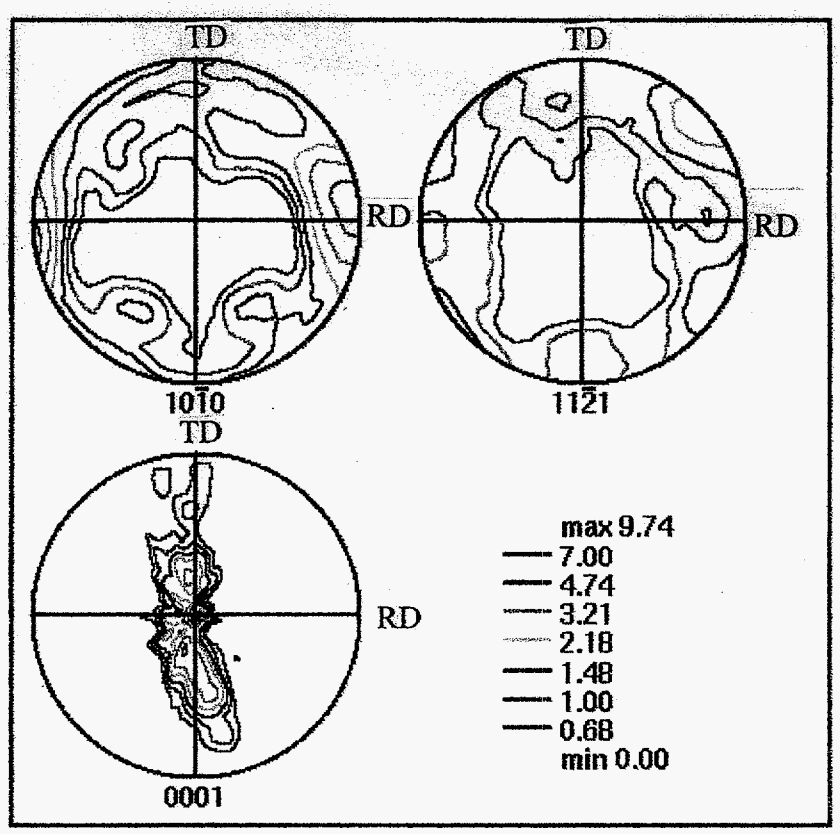

TD - Transverse Direction

RD - Rolling Direction

Figure 6

Zircaloy-4 Test Material Uniaxial Tensile Properties

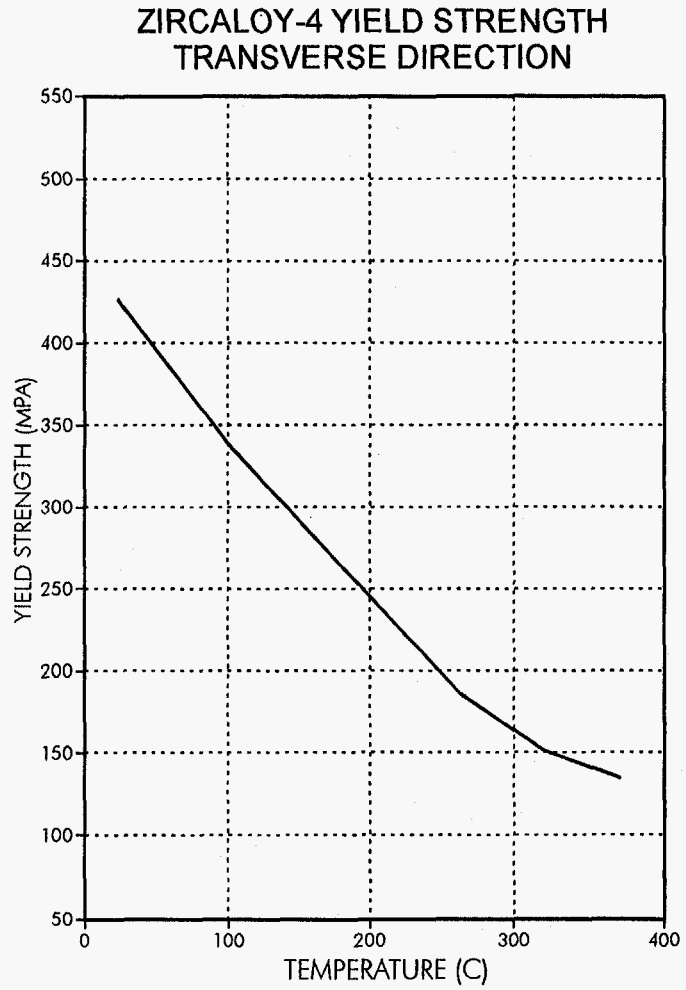

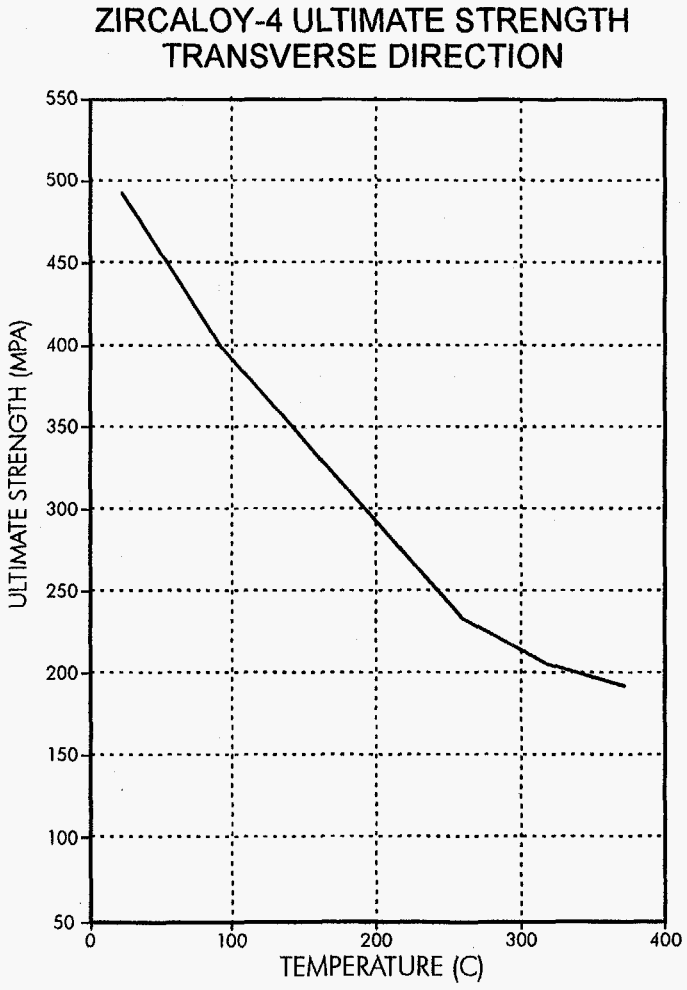

Figure 6 (cont)

Zircaloy-4 Test Material Uniaxial Tensile Properties

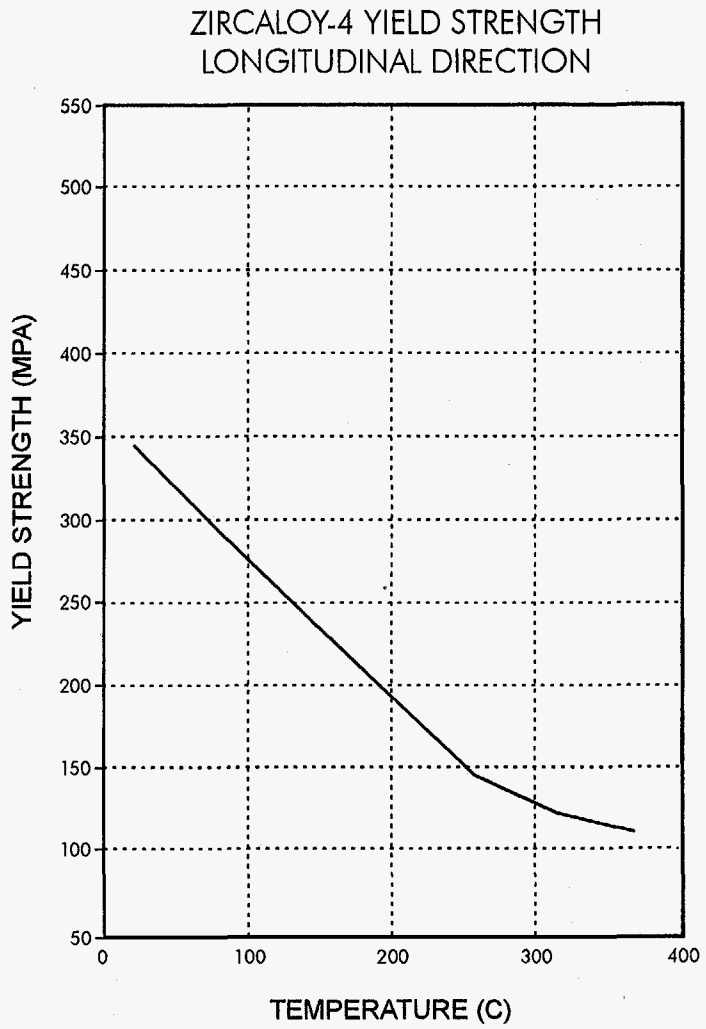

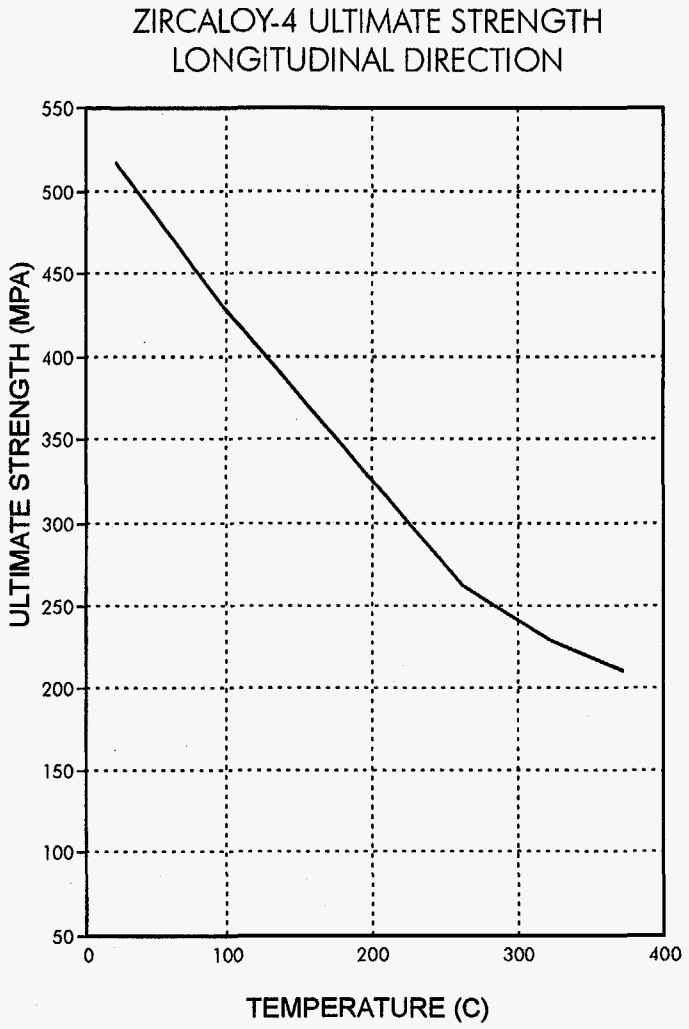

Figure 7

Dog - Bone Applied Compression and Tension Specimens

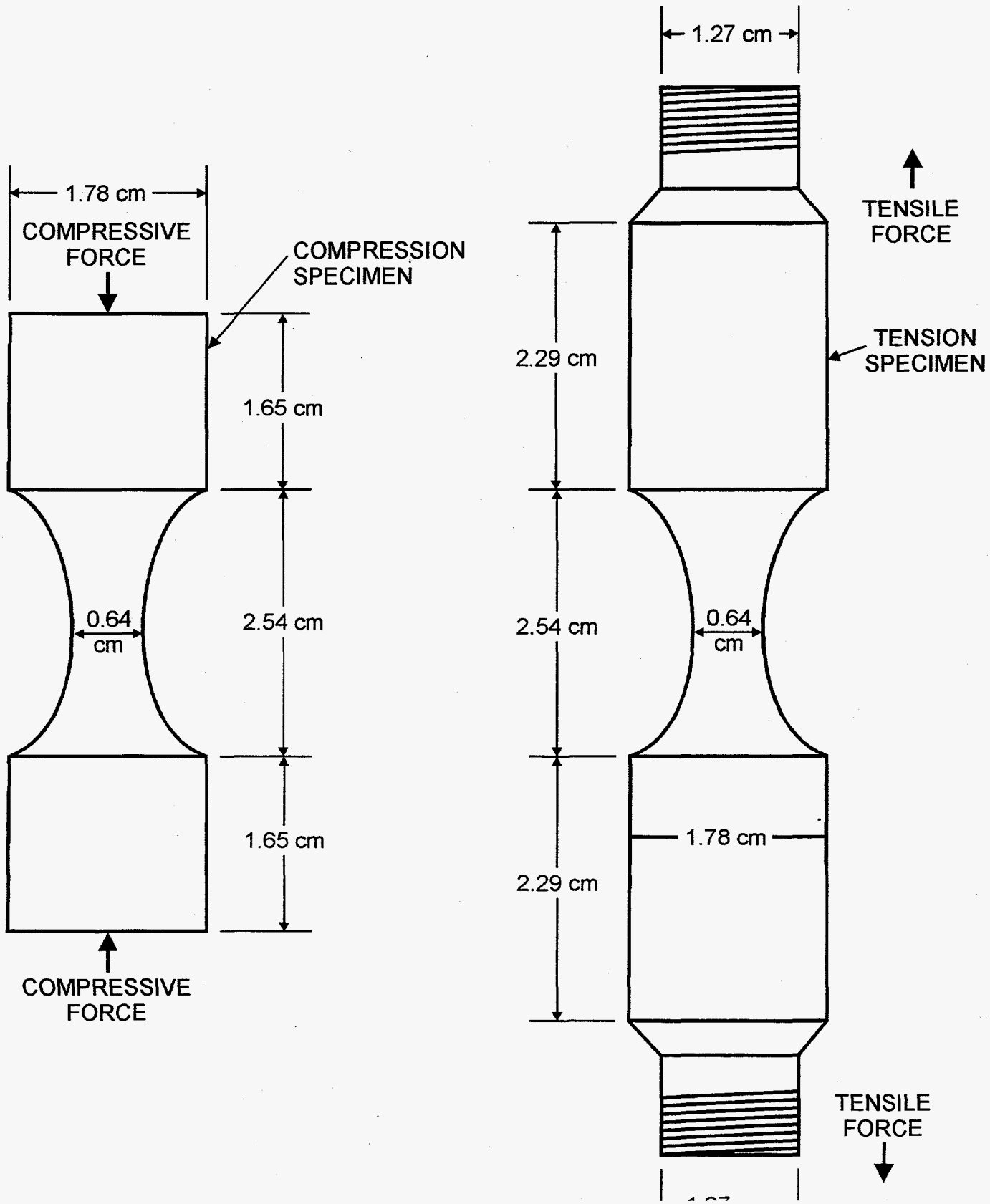

Figure 8

Thermal Cycled Applied Stress Samples

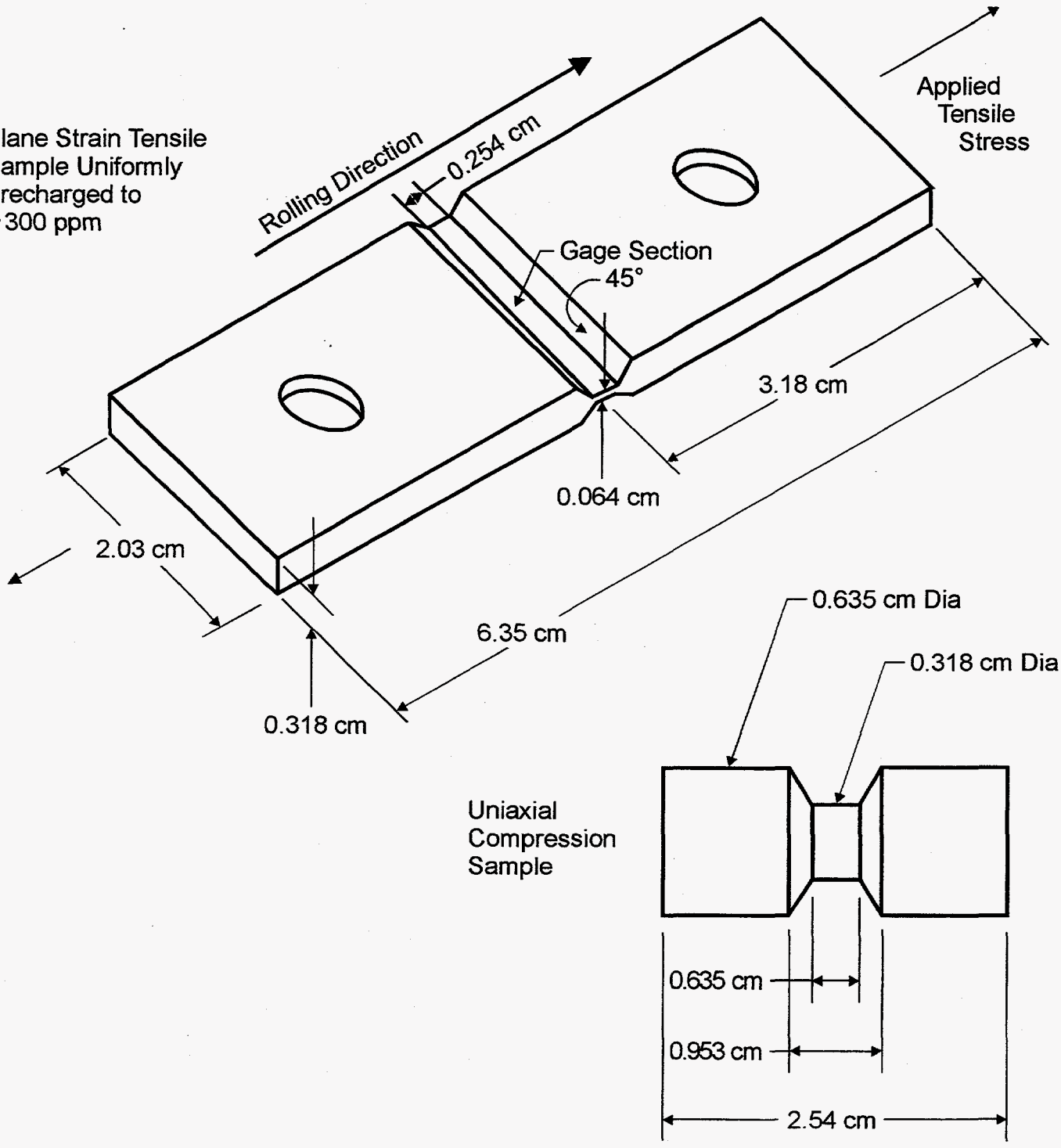

Figure 9

Self Stress Test Specimen

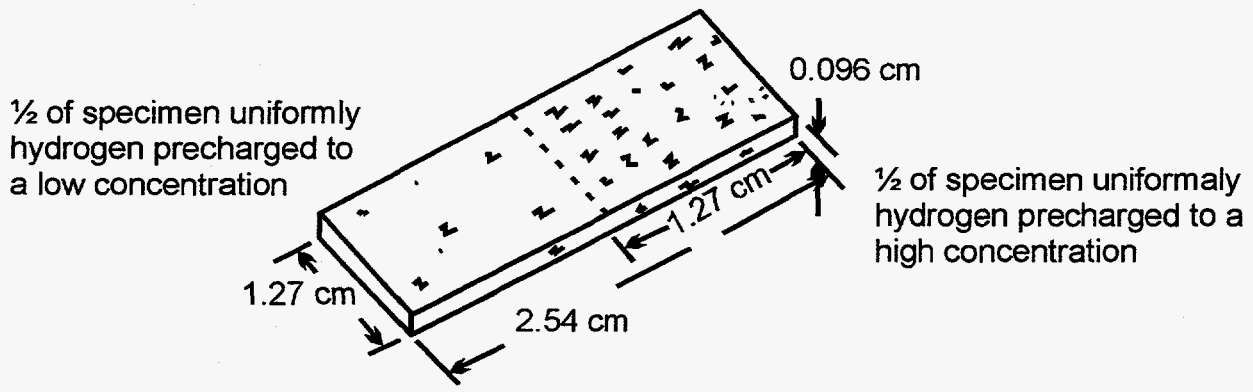

Two Initial Hydrogen Distributions
Employed in Test

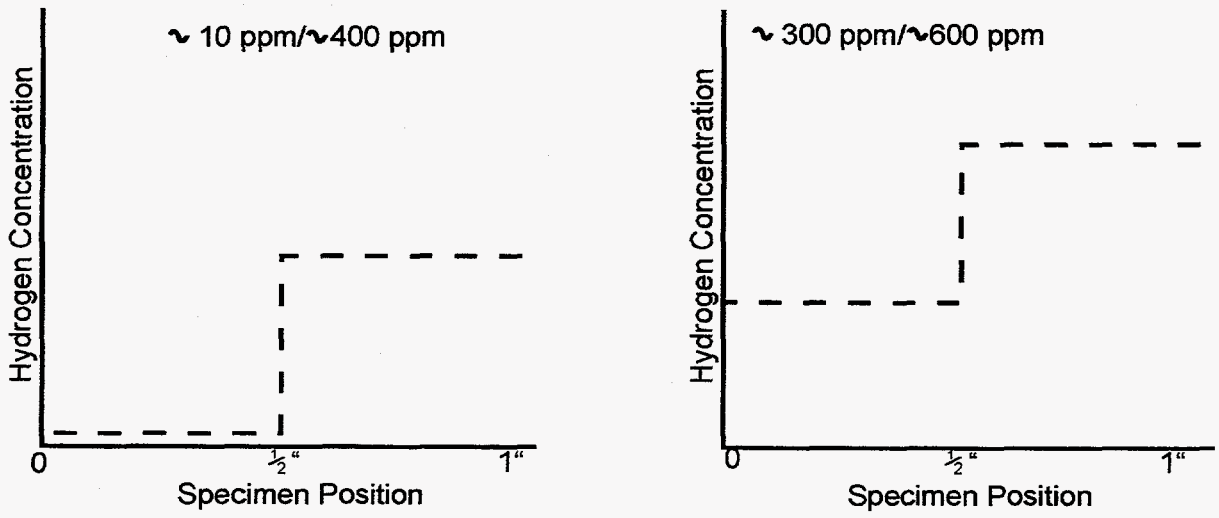

Figure 10

Hydride Layer Thickness vs. Cathodic Charging Time

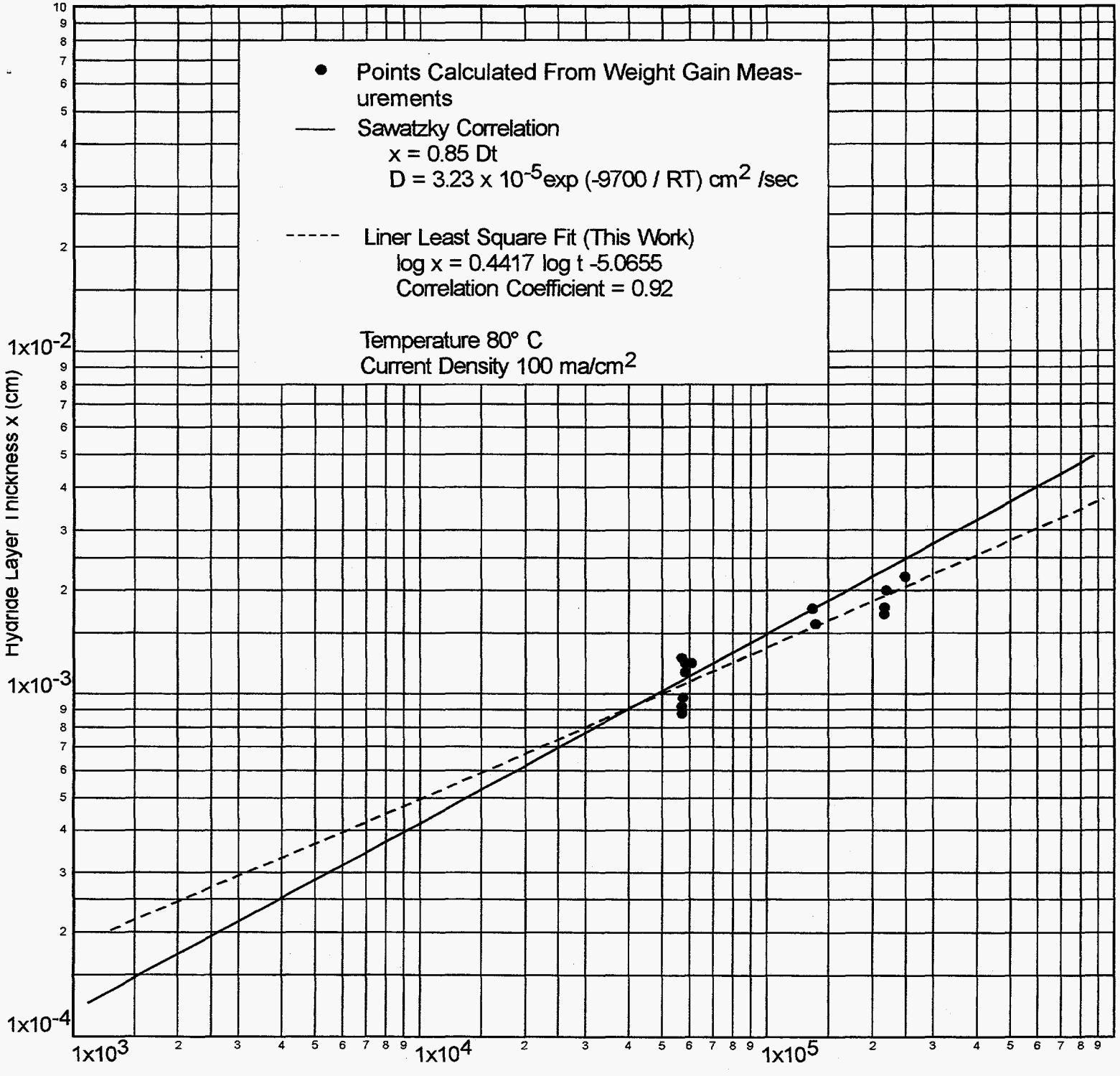

Figure 11

Combined Plane-Strain Applied-Stress/ Thermal Gradient Test Sample

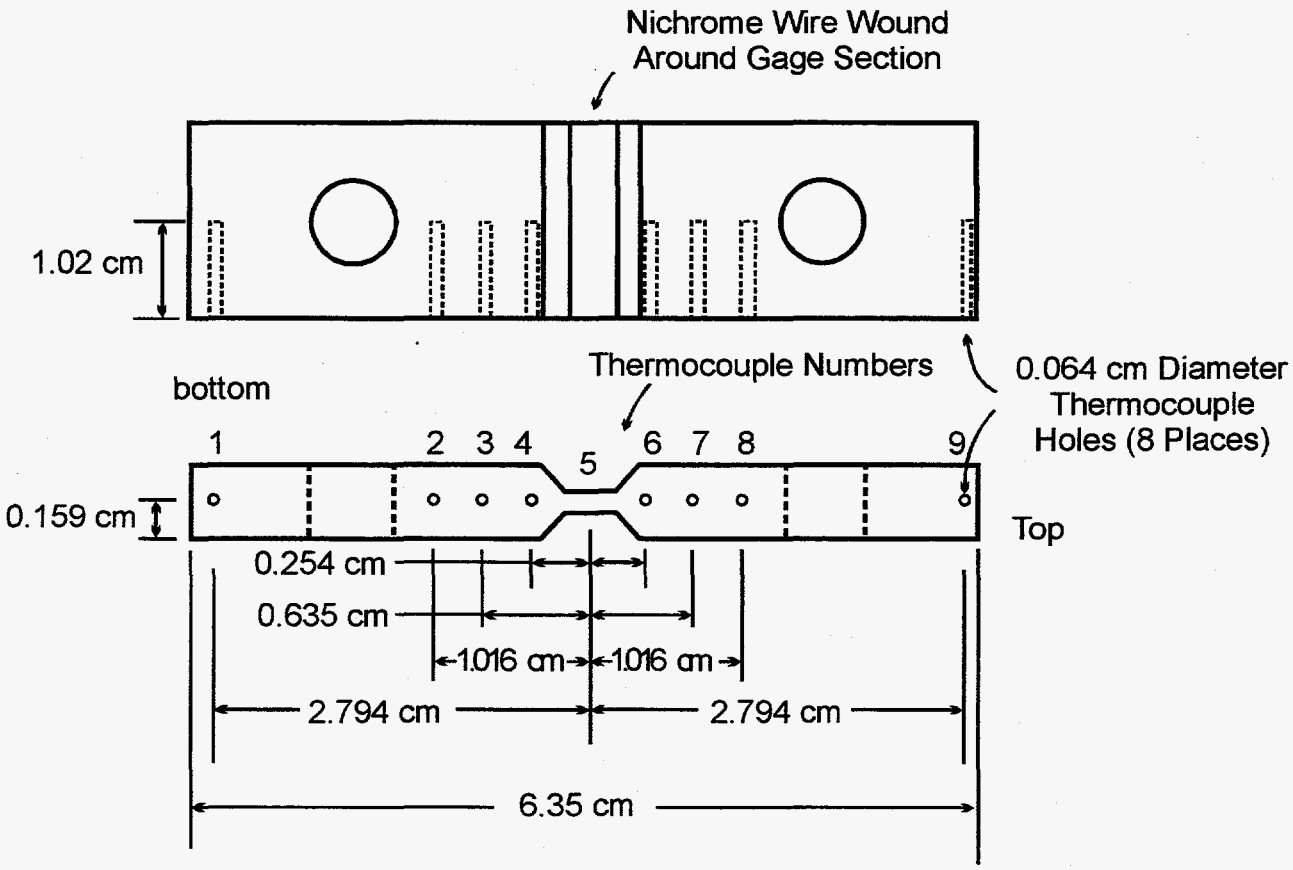

Figure 12

Post Test Sectioning of Samples for Hydrogen Analysis

Sectioning of Dog - Bone Specimens

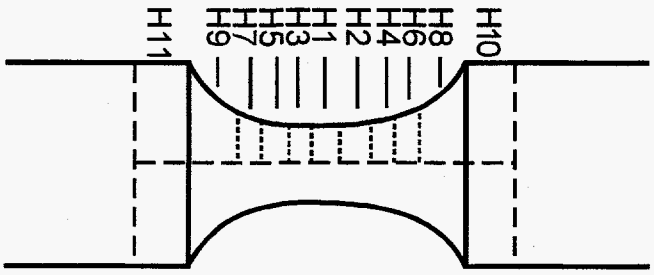

Sectioning of Thermal Cycle Specimens

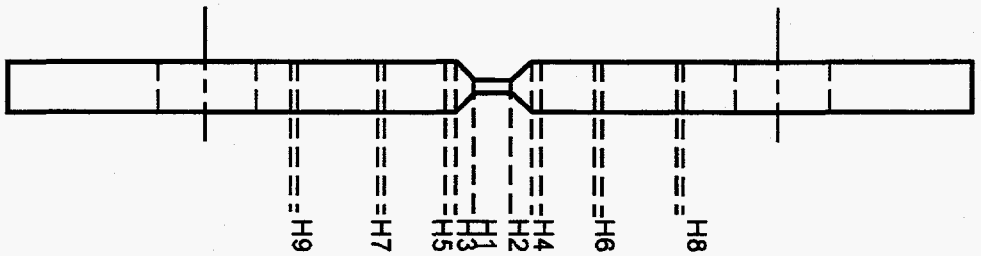

Plane-Strain Tensile

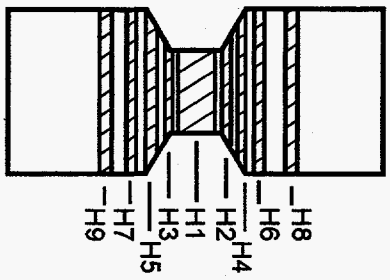

Uniaxial Compression

Sectioning of Self Stress Specimens

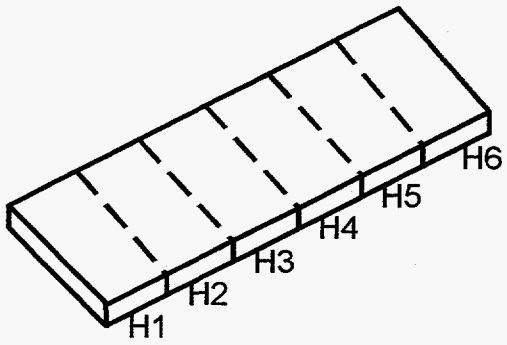

Figure 13

Example of Post - Test Hydrogen Concentrations in Dog - Bone Specimens 316°c,172 Mpa Max Stress, 121 Mpa/cm Stress Gradient

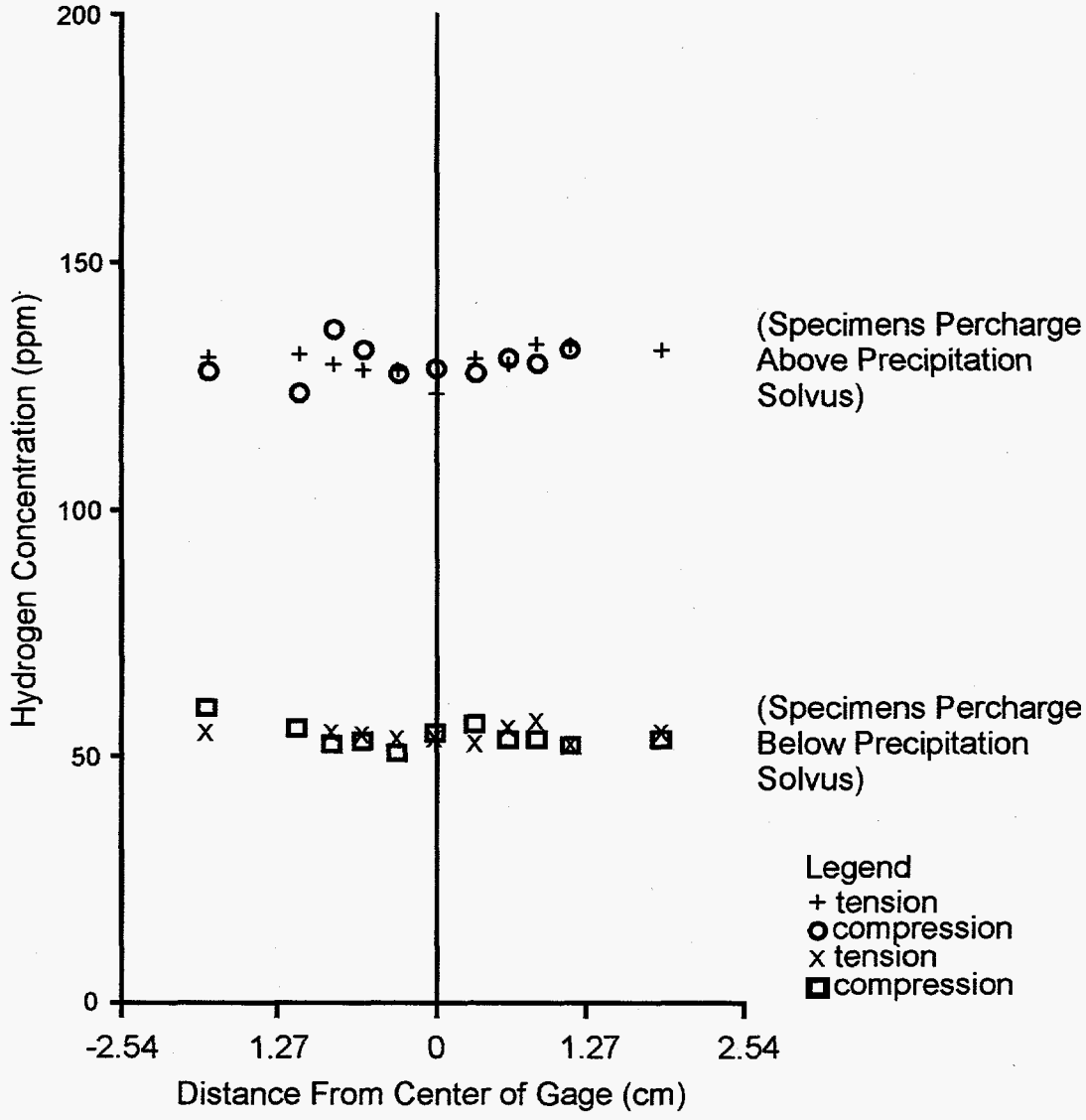

Figure 14

316C, Dog-Bone Sample, 172Mpa Max Stress

Optical Metallography of Post Test Hydrogen Distribution (250X)

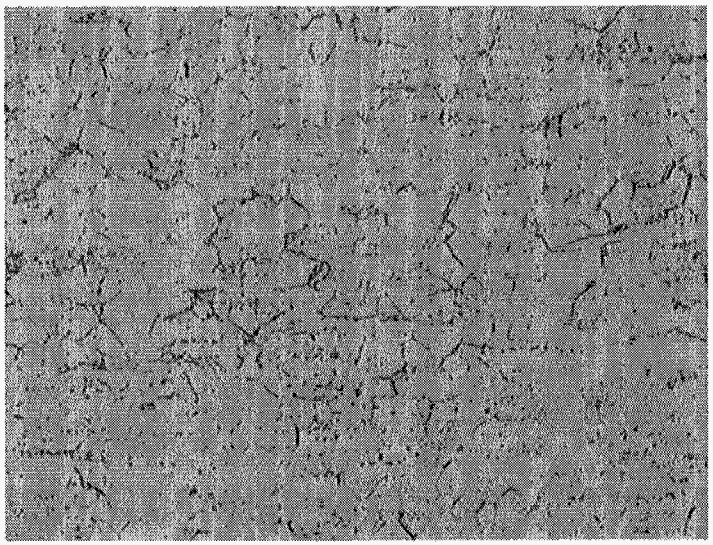

Thin Gage-Section

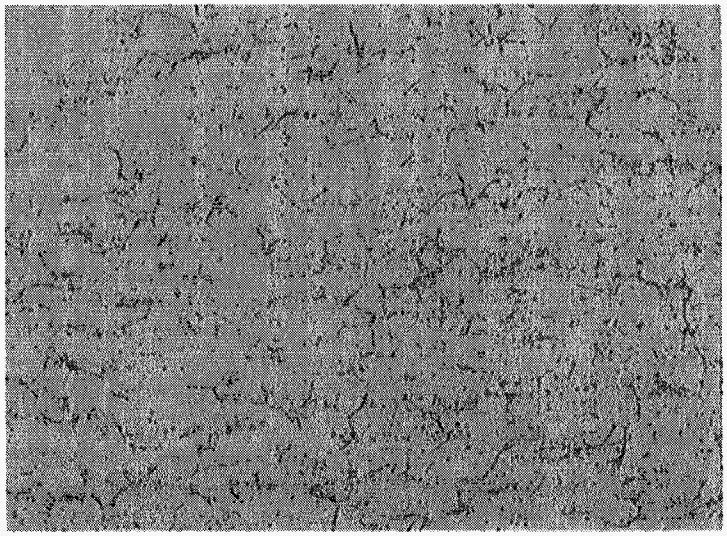

Thick End-Section

Rolling Direction

Figure 15

Example of Post-Test Plane-Strain Hydrogen Concentrations

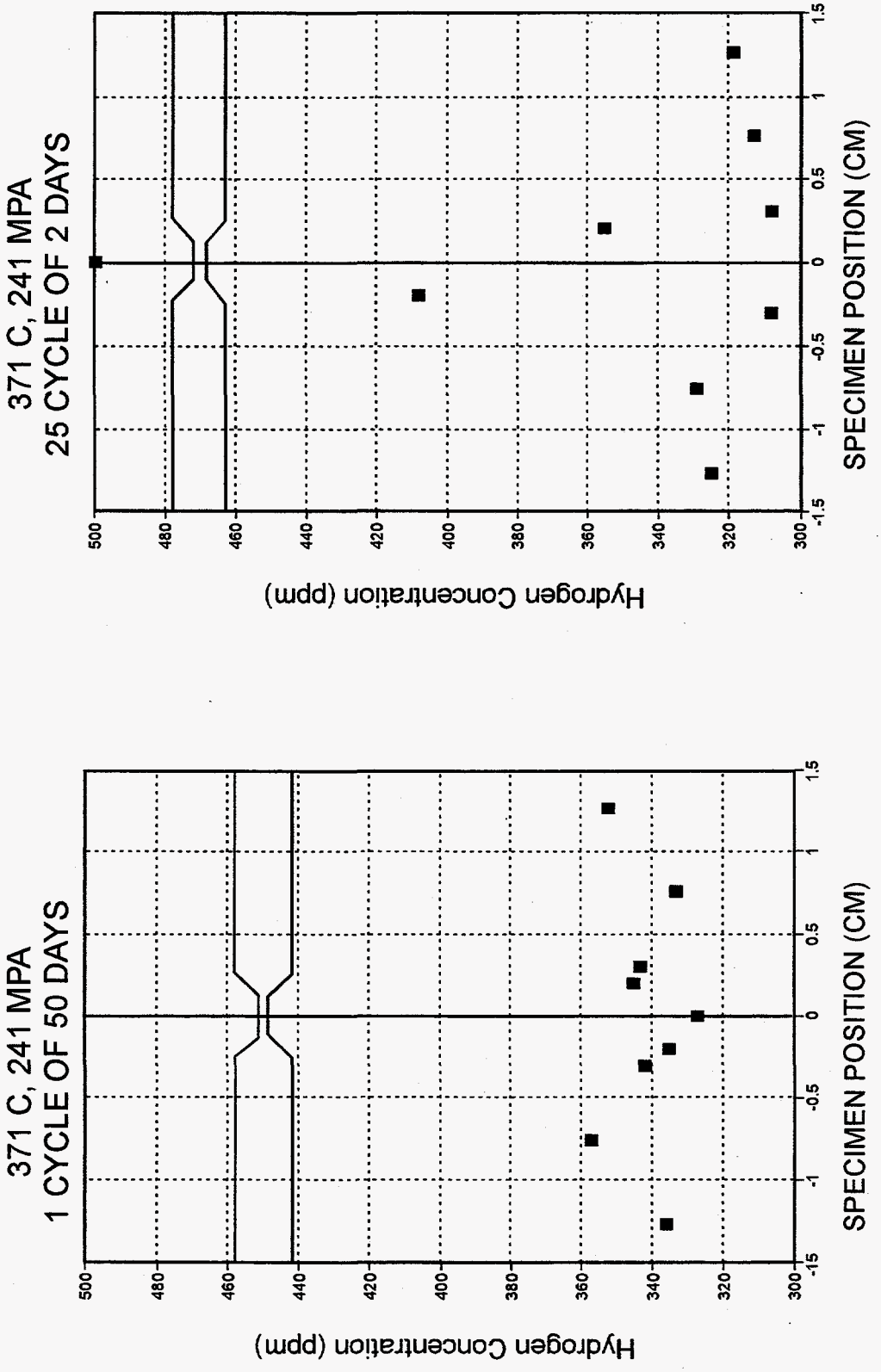

Figure 16

SUMMARY OF STRESS-INDUCED HYDROGEN MIGRATION UNDER THERMAL CYCLING

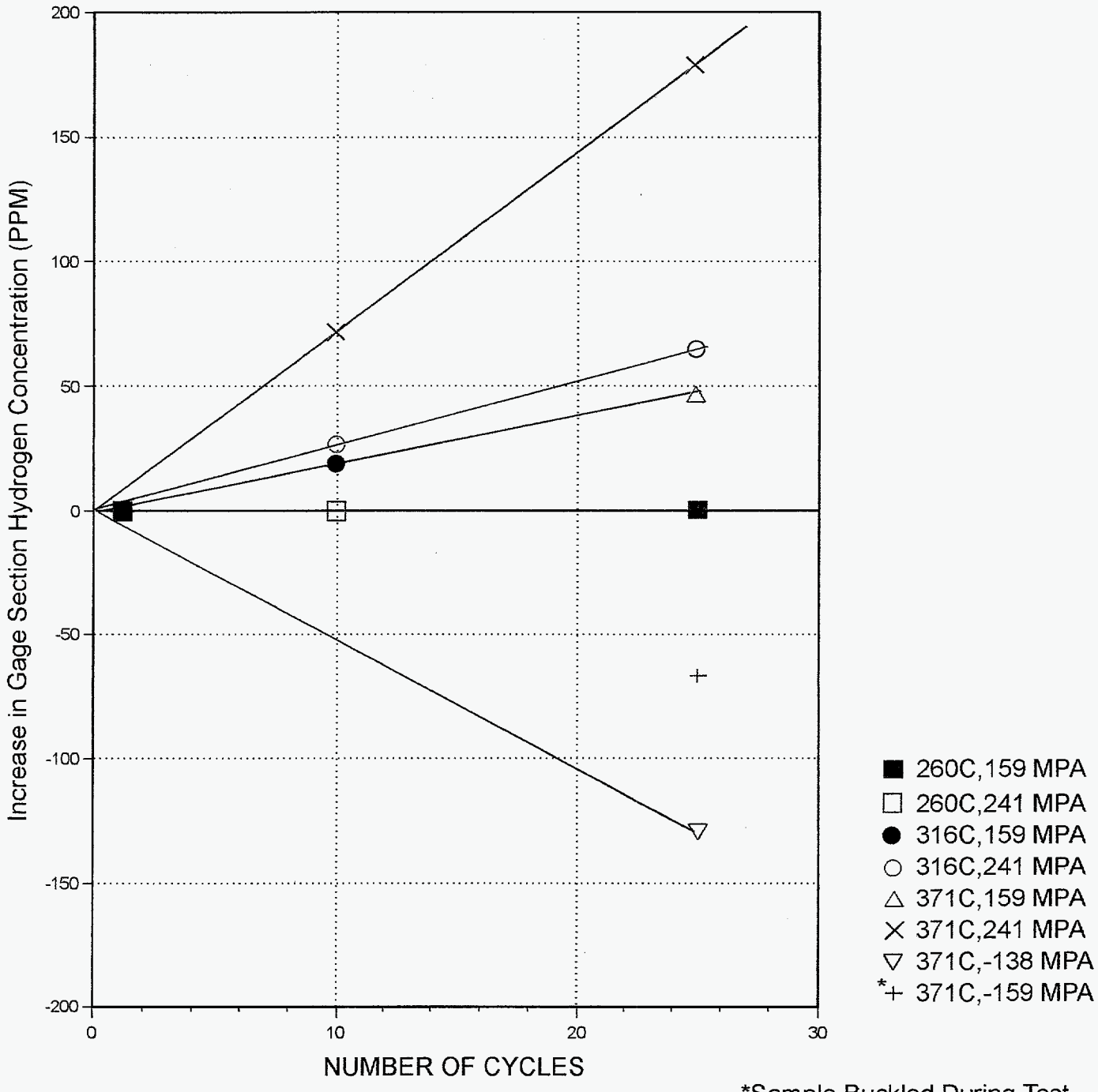

*Sample Buckled During Test

Figure 17

371 C, Thermal Cycle Samples, 240 Mpa

Optical Metallography of Post Test Hydrogen Distribution (250x)

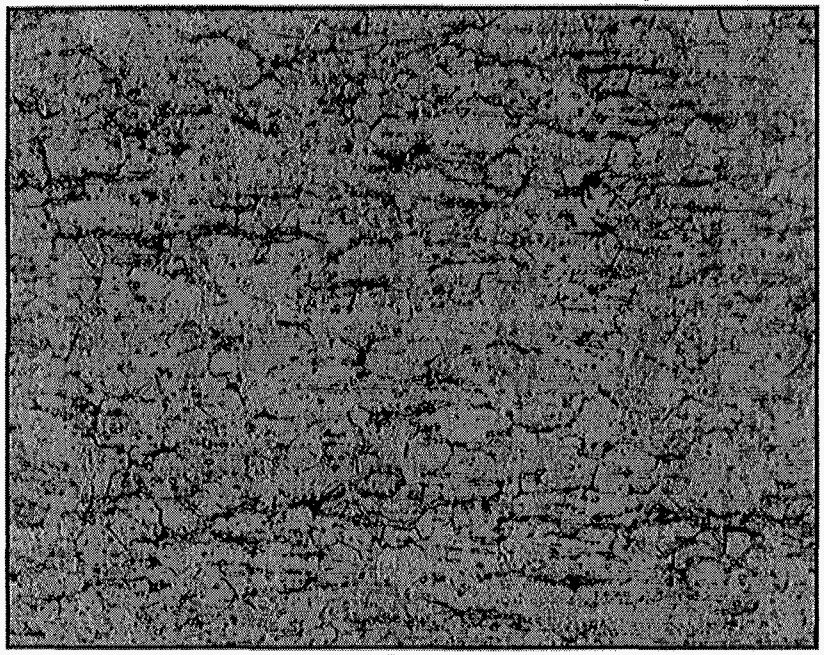

End Section

No Cycles

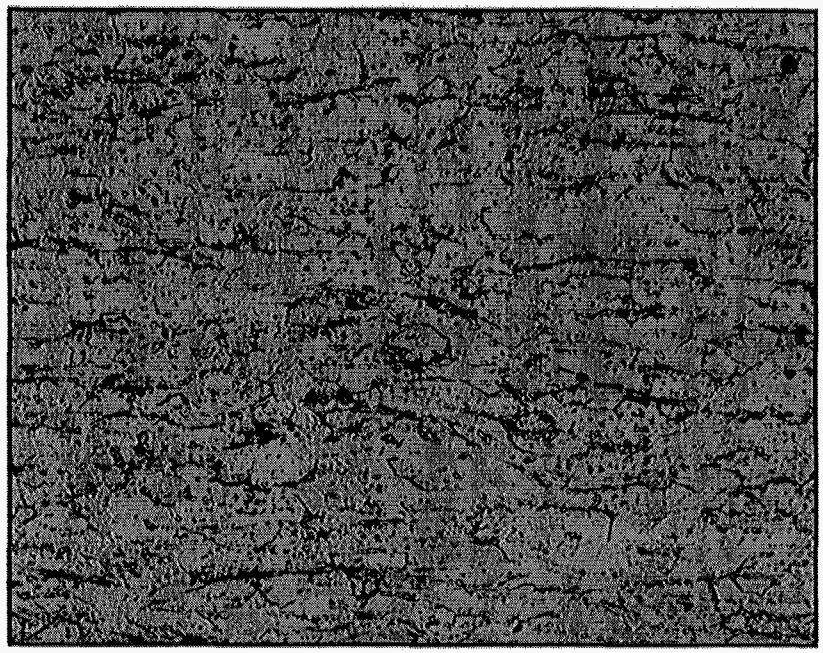

Gage Section

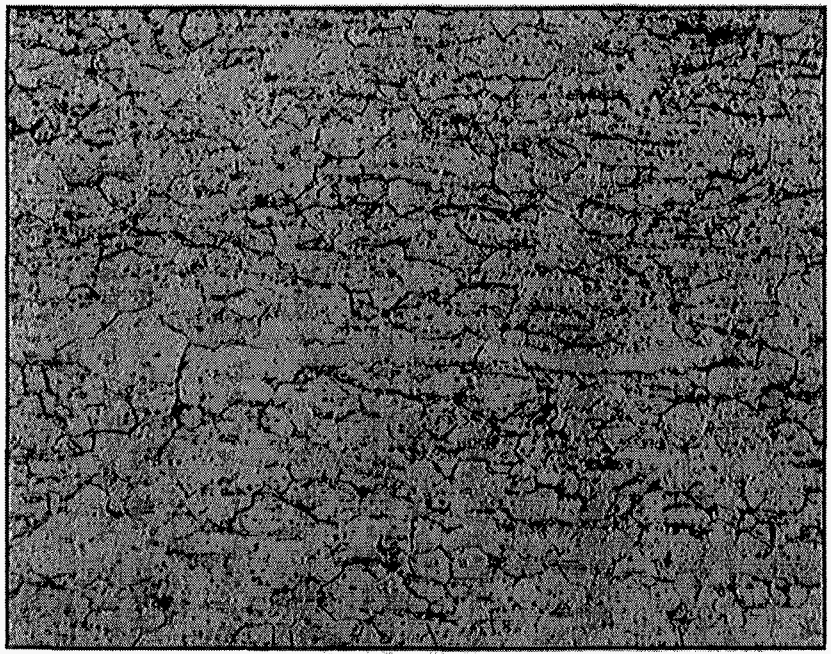

End Section

25 Cycles

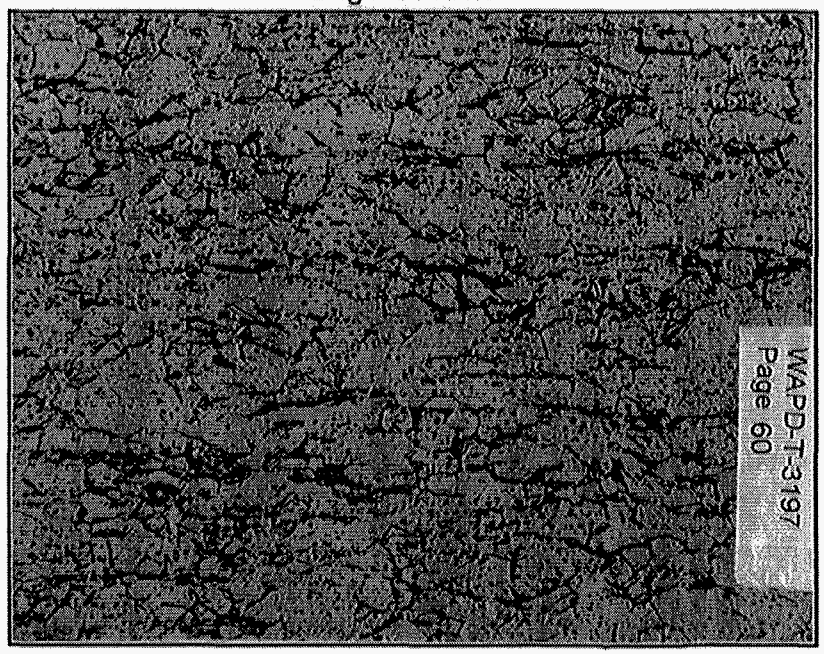

Gage Section

FIGURE 18
Example of Combined Thermal-Gradient/Stress - Gradient Post - Test Hydrogen Concentration Profiles

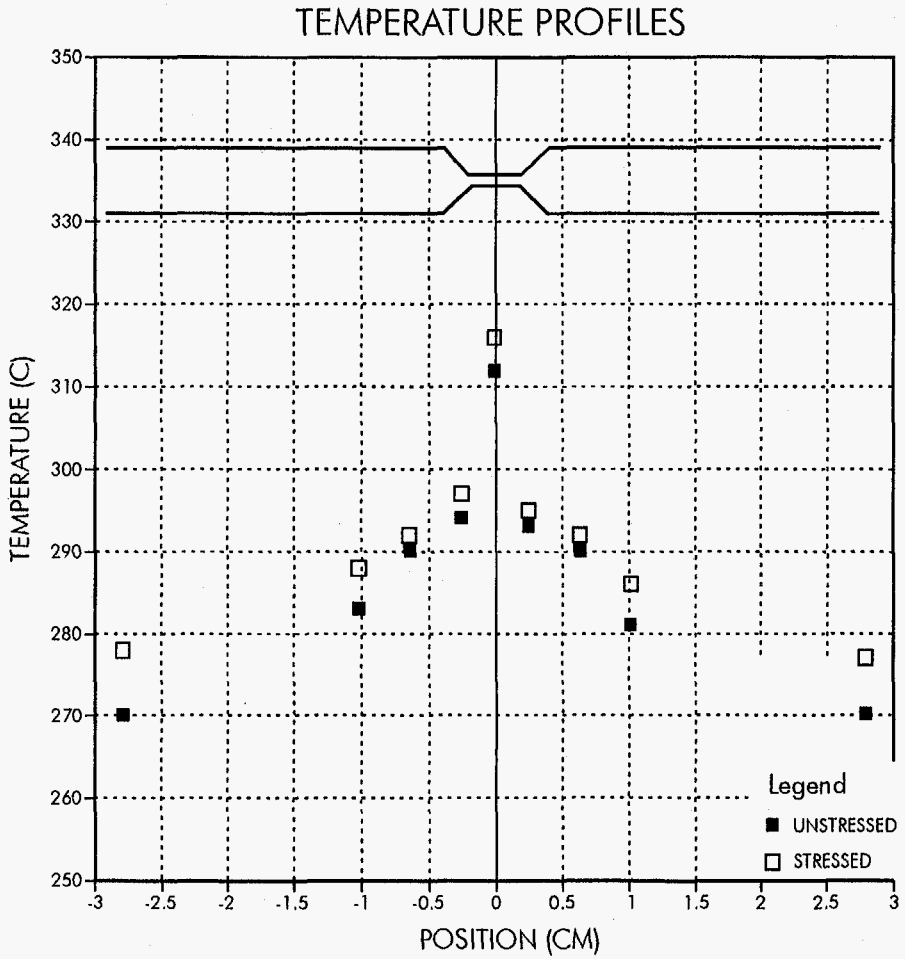

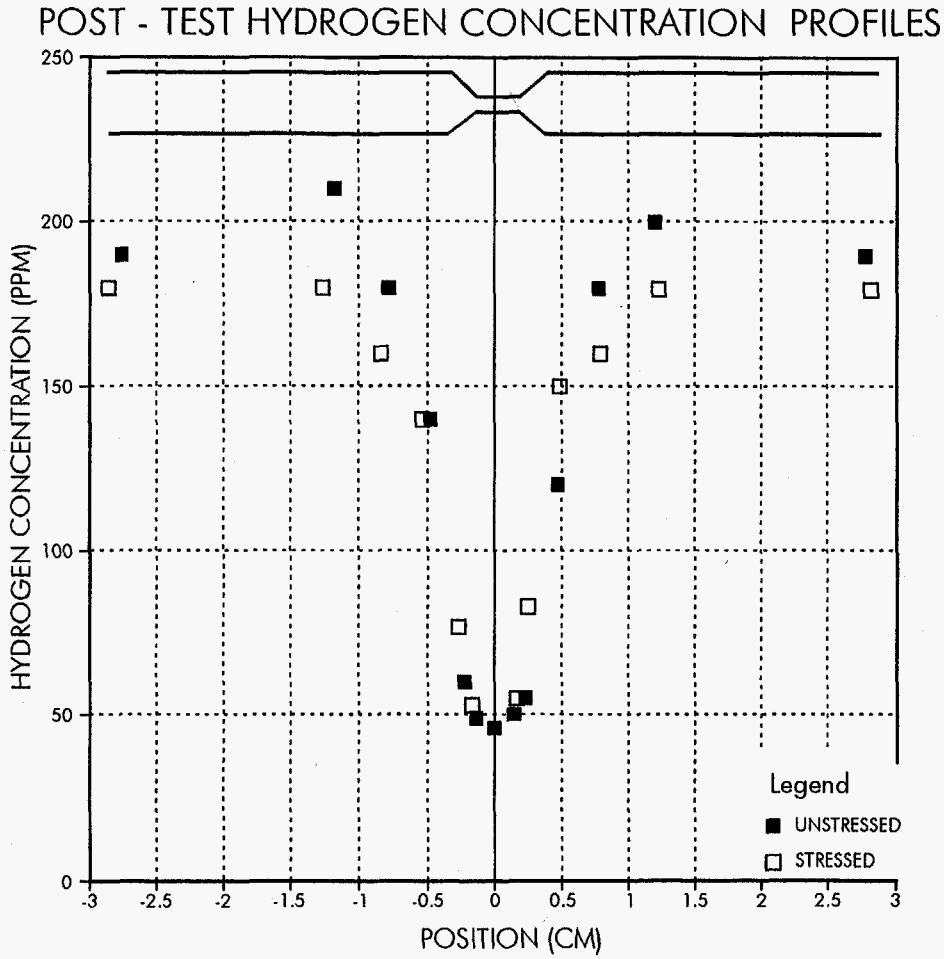

Figure 19

Self - Stress Test Samples
300/600 Diffusion Couple Test Results

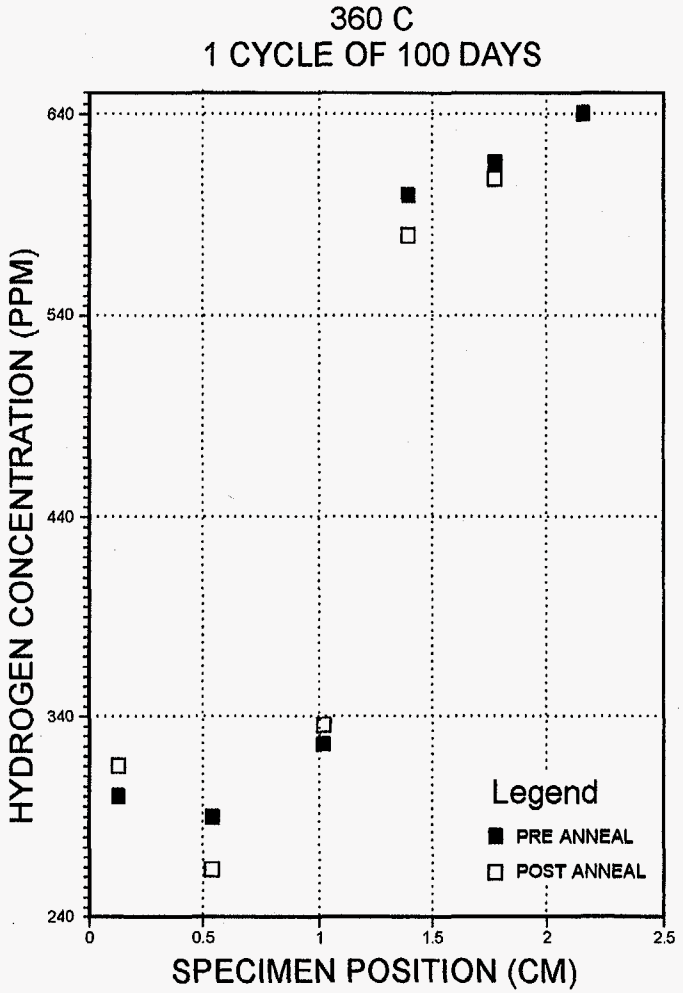

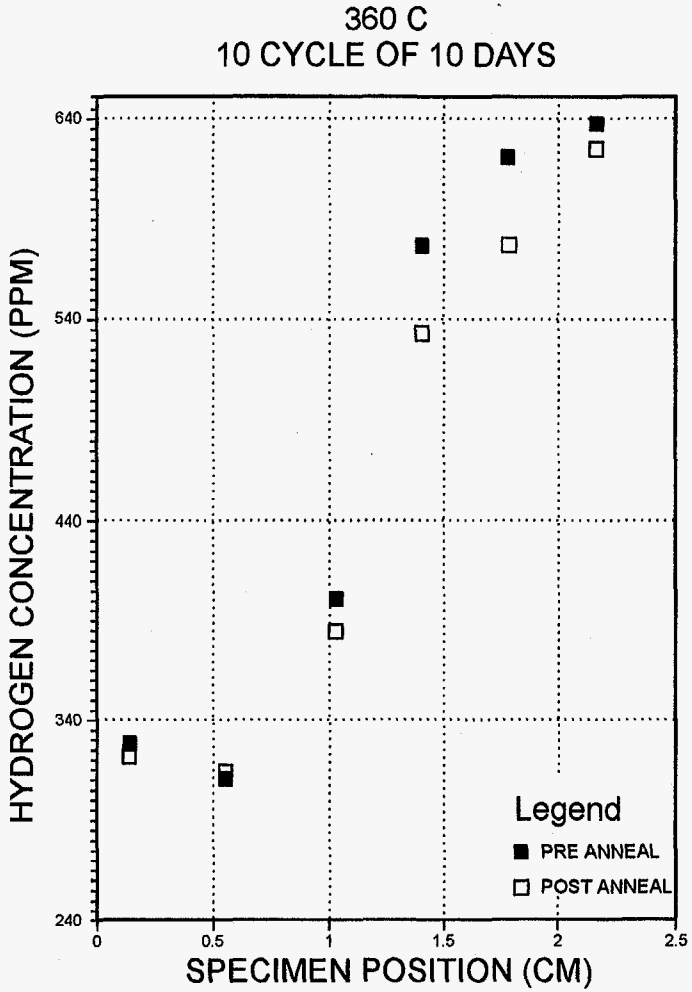

Figure 20

Self - Stress Test Samples
10/400 Diffusion Couple Test Results

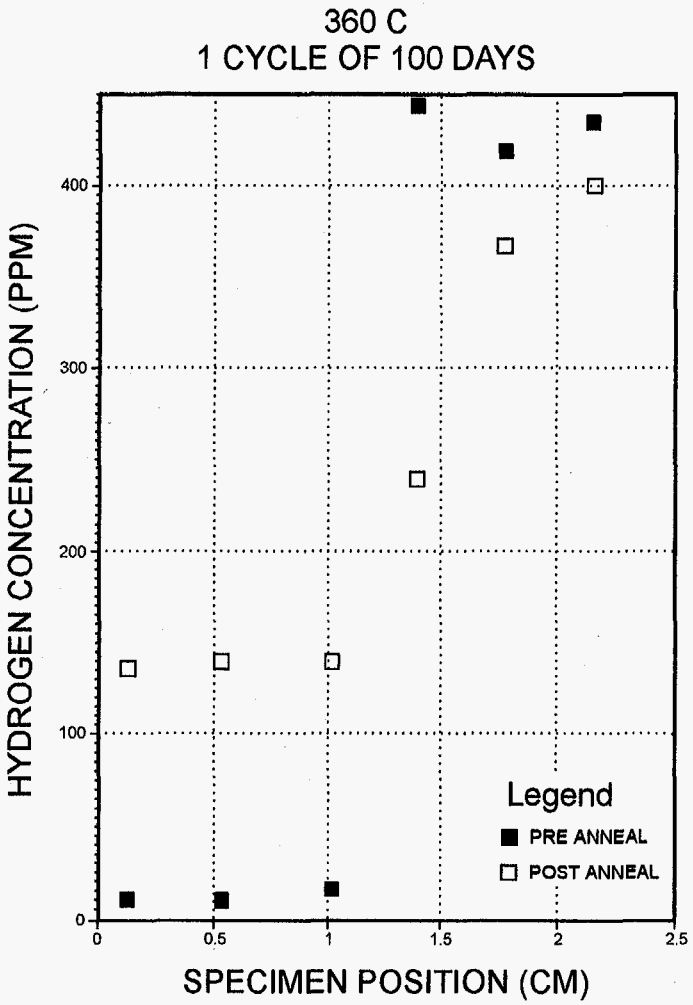

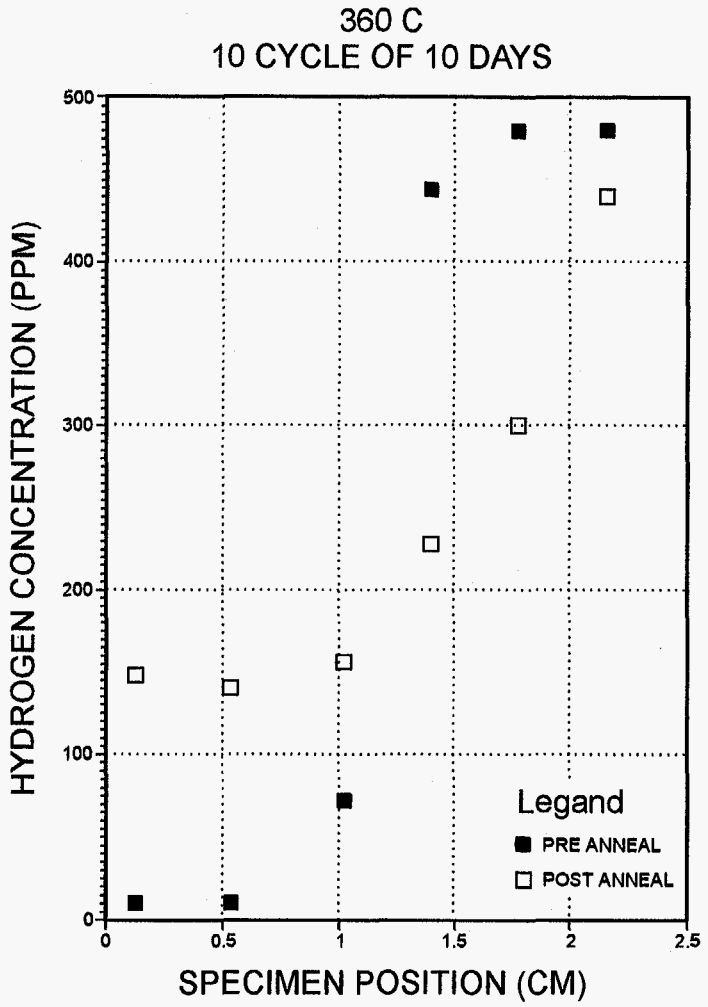

Figure 21

HYDRIDE DISSOLUTION SOLVUS

Comparitive Effect of Temperature and Stress

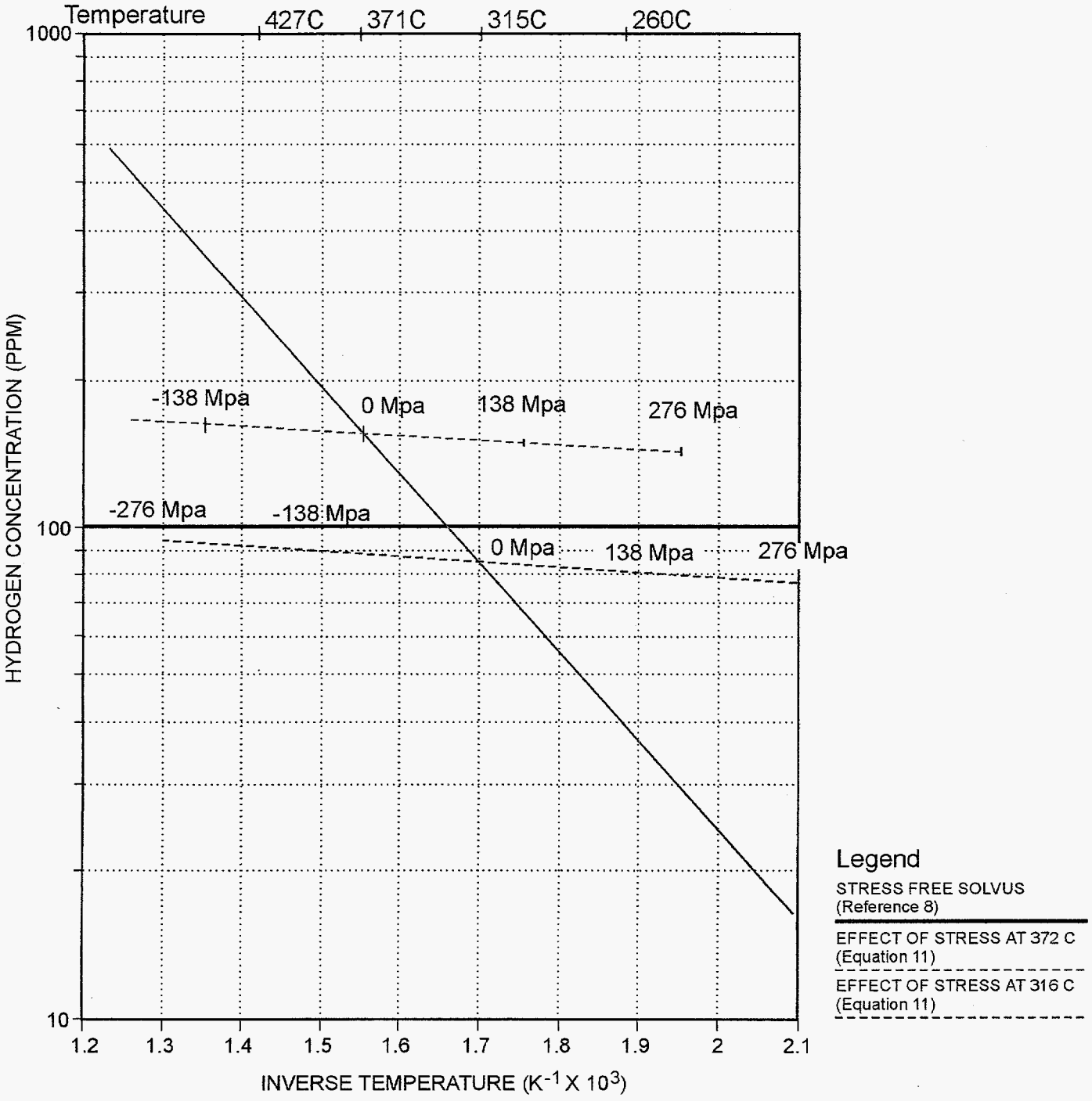

Figure 22

Reference (1) Diffusion Model Calculations of Self-Stress Test Results 360 C, 1 Cycle of 100 Days